

Applied Surface Science

Boudouard reaction under graphene cover on Ni(111)

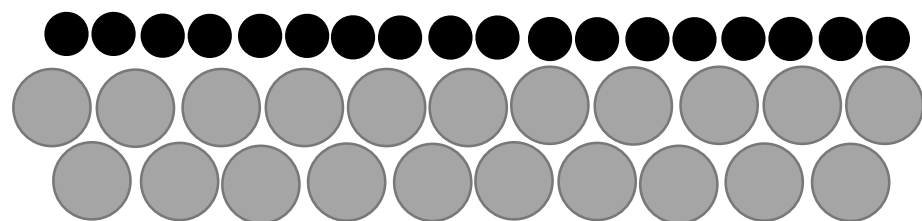
--Manuscript Draft--

Manuscript Number:	APSUSC-D-21-11890R3
Article Type:	Full Length Article
Keywords:	graphene; Chemistry under cover; Boudouard reaction; Near ambient pressure XPS
Corresponding Author:	Luca Vattuone, Ph.D. Università degli Studi di Genova: Università degli Studi di Genova I-16126 Genova, ITALY
First Author:	Rocco Davì, Ph D
Order of Authors:	Rocco Davì, Ph D Giovanni Carraro, Ph D Marija Stojkovska Marco Smerieri, Ph D Letizia Savio, Ph D Mikołaj Lewandowski, Ph D Jean-Jacques Gallet, Ph D Fabrice Bournel, Ph D Mario Rocca, Ph D Luca Vattuone, Ph.D.
Abstract:	We investigated the interaction of CO with graphene/Ni(111) and the Boudouard reaction at 3.7 mbar by Near Ambient Pressure X-Ray Photoemission Spectroscopy (NAPXPS), i.e. at one order of magnitude higher pressure than previously explored in-operando conditions. In this regime, CO intercalates under the graphene layer causing its partial detachment from the Ni substrate. The so-obtained high local CO coverage opens the way to CO ₂ formation via the Boudouard reaction. Its onset is witnessed by observing physisorbed CO ₂ accumulating below the graphene cover. The so-generated additional carbon atoms transform carbide into graphene, causing the expansion of the graphene islands. In addition, CO adsorption occurs on the strongly interacting areas of the graphene layer, confirming previous results obtained by some of us at low temperatures and in ultra-high vacuum conditions.
Suggested Reviewers:	Giovanni Comelli Professor, University of Trieste: Università degli Studi di Trieste giovanni.comelli@elettra.eu Experimentalist with wide experience. Authors of several papers on related topics. Talat Rahman Professor, University of Central Florida talat@ucf.edu Theoretician with wide experience in Surface Science. Authors of a review paper on graphene chemistry. Ado Jorio Professor, Federal University of Minas Gerais: Universidade Federal de Minas Gerais adojorio@fisica.ufmg.br Experimentalist with expertise on graphene.

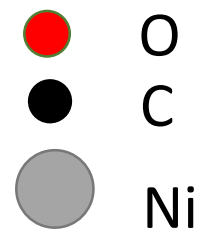
HIGHLIGHTS:

- CO intercalates under full graphene under Near Ambient Pressure (NAP) conditions
-
- CO₂ is produced by the Boudouard reaction under graphene cover already at 340 K
-
- Under NAP weakly adsorbed CO forms above graphene also at room temperature.

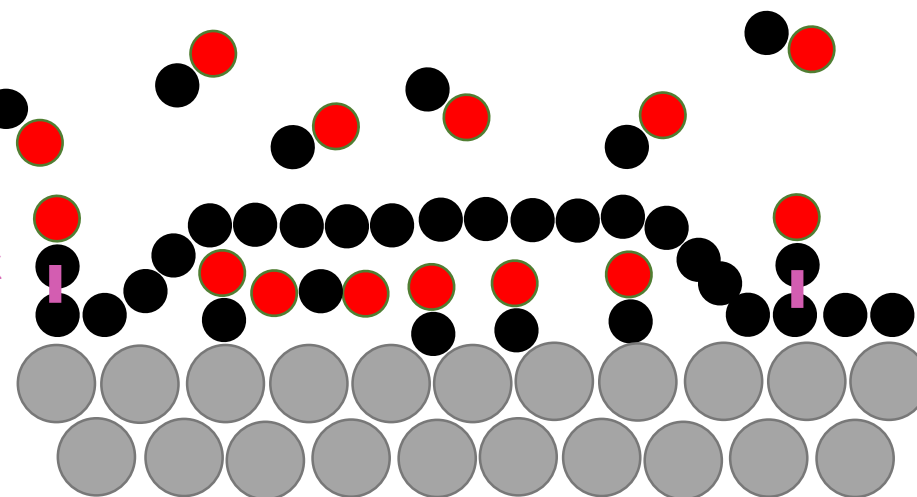
UHV

 $p_{\text{CO}} = 3 \text{ mbar}$ 

G/Ni(111)



CO weak



G/CO/Ni(111)

Boudouard reaction under graphene cover on Ni(111)

Rocco Davì^{1,3}, Giovanni Carraro^{2,3,4}, Marija Stojkowska^{1,3}, Marco Smerieri³, Letizia Savio³,
Mikołaj Lewandowski⁴, Jean-Jacques Gallet^{5,6}, Fabrice Bournel^{5,6}, Mario Rocca^{2,3} and Luca
Vattuone^{2,3*}

1 DCCI, Università degli Studi di Genova, Via Dodecaneso 31, 16146 Genova (Italy)

2 DIFI, Università degli Studi di Genova, Via Dodecaneso 33, 16146 Genova (Italy)

3 IMEM-CNR, UOS di Genova, Via Dodecaneso 33, 16146 Genova (Italy)

4 NanoBioMedical Centre, Adam Mickiewicz University, Wszechnicy Piastowskiej 3, 61-614
Poznań, Poland

5 Sorbonne Université, CNRS, Laboratoire de Chimie Physique Matière et Rayonnement, UMR
7614, Campus Pierre et Marie Curie, 4 place Jussieu, 75252 Paris Cedex 05, France

6 Synchrotron SOLEIL, L'Orme des Merisiers, Saint-Aubin, F-91192 Gif-sur-Yvette, France

* Corresponding author. Tel: +39 010 353 6554 <mailto:vattuone@fisica.unige.it>

Abstract

We investigated the interaction of CO with graphene/Ni(111) and the Boudouard reaction at 3.7 mbar by Near Ambient Pressure X-Ray Photoemission Spectroscopy (NAPXPS), i.e. at one order of magnitude higher pressure than previously explored in-operando conditions. In this regime, CO intercalates under the graphene layer causing its partial detachment from the Ni substrate. The so-obtained high local CO coverage opens the way to CO₂ formation via the Boudouard reaction. Its onset is witnessed by observing physisorbed CO₂ accumulating below the graphene cover. The so-generated additional carbon atoms transform carbide into graphene, causing the expansion of the graphene islands. In addition, CO adsorption occurs on the strongly interacting areas of the graphene layer, confirming previous results obtained by some of us at low temperatures and in ultra-high vacuum conditions.

KEYWORDS

Graphene, Chemistry under cover, Boudouard reaction, Near Ambient Pressure XPS

1. Introduction

Nowadays, graphene (G) growth is routinely obtained on reactive substrates by hydrocarbon dehydrogenation at high sample temperatures. However, the presence of the substrate affects the transport properties of the G layer. In the case of strongly interacting substrates, such as G/Ni [1,2] and G/Ru [3], the Dirac cone is destroyed or shifted, and, consequently, the exceptional mobility of the charge carriers is lost. A promising way to decouple G from the underlying substrate and restore its peculiar electronic properties is the intercalation of atoms [4] and molecules [5], which has been thoroughly investigated.

Confinement of molecules under the G layer is also interesting for sensoristics and catalysis. On the one hand, the change in the electronic properties of graphene can be used as a probe of adsorption [2]; on the other hand, chemical reactions may be affected by the spatial confinement of the reactants. E.g., the G overlayer weakens the interaction between CO and Pt(111), thus reducing the activation barrier for its oxidation [6]. Therefore the interfaces between G and metal surfaces may act as 2D confined nanoreactors, in which catalytic processes are promoted [7]. The feasibility of this approach was also demonstrated for CO oxidation on G-covered Pt nanoparticles [8] and methanation on h-BN-covered Ni nanoparticles [9].

An experimental study of CO intercalation under G/Ni(111) has been recently performed by Wei et al. by Near Ambient Pressure X-ray Photoemission Spectroscopy (NAPXPS) [10,11] in-operando conditions up to 0.1 Torr. Exposure to 5 Torr has been reported as well, but XPS inspection was performed only after the evacuation of the experimental chamber. The authors find that CO intercalation occurs under a complete G layer, with CO ending up mainly at bridge positions with only a minor component at atop sites. Therefore they conclude that, under the G cover, CO behaves similarly on a bare Ni(111) surface under Ultra High Vacuum (UHV) conditions and at room temperature (RT) [12]. Upon annealing, partial deintercalation of CO occurs at ~350 K. Still, a significant amount of intercalated CO persists even after annealing to 473 K. As expected, the initially strongly interacting G layer detaches from the substrate due to intercalation, giving rise to graphene patches characterised by components at a lower binding energy in the XPS spectrum (weakly interacting and detached graphene in the following). More importantly, no additional O-containing species were detected, neither upon CO intercalation nor during the subsequent in-vacuum annealing procedure.

1 In a recent paper, we presented experiments performed at the Tempo Beamline of the Soleil
2 Synchrotron radiation source, demonstrating that G can be grown on Ni(111) by CO exposure at NAP
3 conditions and at T=500 K, i.e. at a temperature significantly lower than the one needed when using
4 hydrocarbons as C source [13]. In that study, we also evidenced the first CO₂ formation via the
5 Boudouard reaction above T=600 K. This paper reports on complementary results obtained at the
6 same facility by performing in-operando NAPXPS experiments. In this experiment, a full G/Ni(111)
7 layer is grown by ethene dehydrogenation, and it is exposed to CO at a pressure as high as 4 mbar.
8 We demonstrate that CO intercalates and allows for the onset of the Boudouard reaction already at
9 340 K, leading to CO₂ accumulation under the G cover. New physics is therefore disclosed by
10 exploring this so far untrodden pressure range.
11
12
13
14
15
16
17
18
19
20

21 **2. Methods**

22 **2.1 Experimental Set-up**

23 The experiments were performed at the TEMPO beamline of the SOLEIL Synchrotron Radiation
24 source (Saint-Aubin, France) with the NAPXPS facility of Sorbonne Université. The experimental
25 setup is described in detail in ref [14], so we only recall the experimental features pertinent to the
26 present work.
27
28
29
30
31
32
33

34 The setup allows measurements from UHV conditions up to 20 mbar. Synchrotron Radiation enters
35 through a differentially pumped stage, forming a beam of 0.1 mm diameter that strikes the sample at
36 an angle of 54° with respect to the surface normal. In NAP conditions, the attenuation of the
37 photoemission signal by scattering off gas-phase CO depends exponentially on the distance between
38 the sample surface and the analyser collimator. Thus the sample is kept at ~1 mm distance from the
39 collimator to limit this attenuation. To keep the pressure in the main chamber as constant as possible
40 during NAP experiments, all connections to the pumping systems are sealed by valves. The residual
41 pumping action of nozzle and beam entrance holes is compensated by letting in some CO via a leak
42 valve.
43
44
45
46
47
48
49
50

51 **2.2 Sample preparation**

52 The Ni crystal is mounted on a sample holder heated by a ceramic heater module. The Ni(111) surface
53 is cleaned in UHV by sputtering cycles with 3 keV Ar⁺ ions followed by annealing to T~1000 K and
54 by reactive cleaning in 5·10⁻⁷ mbar of O₂ at 1000 K for 10 minutes. This procedure led to a surface
55 clean of contaminants but some carbide, which could not be removed entirely.
56
57
58
59
60
61
62
63
64
65

1 Graphene was grown by exposing the sample at $T=830$ K to $P=1.7 \cdot 10^{-5}$ mbar of C_2H_4 for 300 s,
2 corresponding to ~ 3800 L, i.e. following the same protocol as in ref. [15].
3

4 Selected spectra of the C 1s region recorded during the growth process are shown in Fig. 1. The
5 bottom spectrum (black) corresponds to the surface at RT after completing the cleaning procedure.
6 We note that it still shows some nickel carbide, which could not be removed. The sample is eventually
7 heated to 830 K and exposed to C_2H_4 (green spectra). Then the chamber is evacuated while keeping
8 the sample at 825 K (dark green spectrum), and the latter is eventually cooled down at 450 K under
9 UHV conditions (topmost blue spectrum). The formation of graphene is indicated by the appearance
10 of a peak centred around 284.5 eV. We notice that its intensity is lower at the end of the exposure
11 (dark green trace) than after cooling the sample (blue trace). This indicates that, while most of the G
12 layer forms by ethene dehydrogenation, full monolayer coverage is reached by C segregation during
13 the cooling process. A more detailed inspection of the data shows that the relevant temperature for
14 segregation ranges from $T=830$ K to 580 K, while no further changes occur in the C 1s spectral region
15 at lower T.
16
17
18
19
20
21
22
23
24
25
26
27
28
29
30
31
32
33
34
35
36
37
38
39
40
41
42
43
44
45
46
47
48
49
50
51
52
53
54
55
56
57
58
59
60
61
62
63
64
65

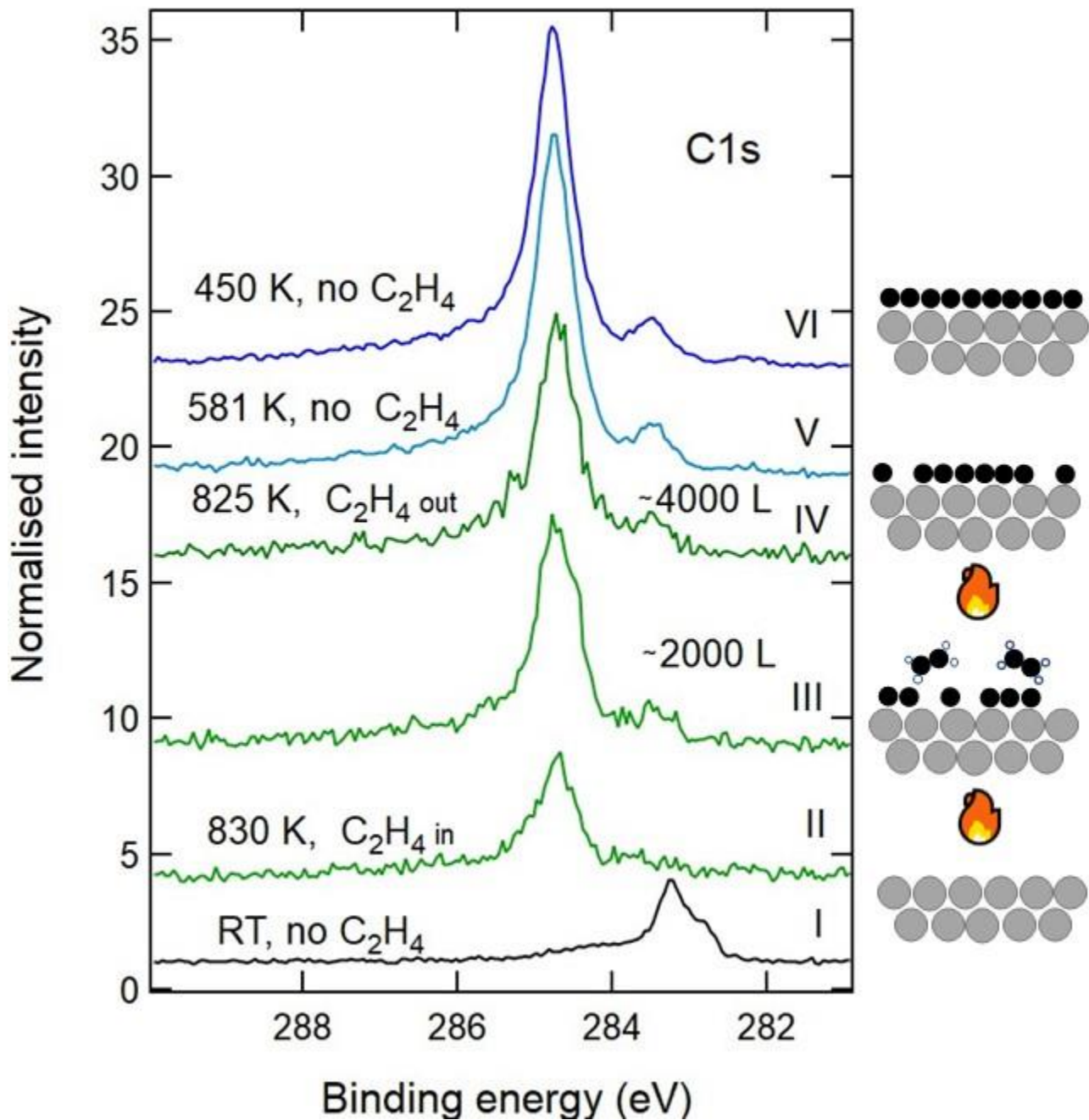


Fig.1 Evolution of the C 1s region during graphene growth by ethylene dehydrogenation. Spectra were recorded with photon energy $h\nu=400$ eV to achieve a high sensitivity to carbon. Spectra are normalized scaling the value of the background in the low binding energy region to 1. From bottom to top: I) Ni(111) surface at RT after the cleaning procedure. Some residual nickel carbide is still present, and it transforms into graphene upon heating between 640 K and 716 K. The low E_b shoulder of the Ni₂C peak is due to a carbon deficient carbide phase [10]. II) Spectrum recorded with the sample at $T=830$ K, just after admitting C₂H₄ into the chamber. III) Same as II) after about 150 s exposure. IV) Spectrum recorded at $T=825$ K after the evacuation of the chamber. The total exposure time to ethylene was 300 s. V) Spectrum recorded at 581 K while cooling the sample in UHV. VI)

1 Spectrum recorded at T=450 K. The total carbon coverage in VI is 1.45 ML_{Ni(111)} (out of which 1.26
2 ML_{Ni(111)} is graphene, and 0.19 ML_{Ni(111)} is Ni₂C). The sketches on the right schematise the different
3 stages of the experiment.
4
5
6
7

8 **2.3 Fitting procedure of the XPS spectra.** 9

10 Unless otherwise specified, XPS spectra of the C 1s and O 1s regions were performed at the photon
11 energy $h\nu=650$ eV, while $h\nu=970$ eV was used for the Ni 2p region (not shown, recorded for control
12 purpose only).
13
14
15

16 XPS analysis was performed with the KOL-XPD software. All binding energies (E_b) are calibrated
17 with respect to the Fermi edge of the Ni sample, which was acquired as a reference for each set of
18 experiments. After subtracting a Shirley background, the main C 1s peak (related to graphene) has a
19 strong asymmetry and is therefore fitted with Doniach-Sunjic functions convoluted with a Gaussian.
20 Voigt functions proved sufficient to describe the C1s contributions of CO₂ and of gas phase CO as
21 well as all peaks in the O 1s region. A linear background was used for the O 1s region. All the fitting
22 parameters are detailed in Table S1 of the Supporting Information.
23
24
25
26
27
28
29

30 Following previous literature, we considered the C1s intensity as composed of several lines. The
31 corresponding binding energies are collected in Table I and are considered fixed parameters in the
32 present analysis. The C1s region is dominated by the graphene signal. Graphene interacts strongly
33 with Ni(111), and different domains form depending on the relative position of the G lattice with
34 respect to the one of Ni(111) [16]. In the present experimental conditions, top-bridge graphene
35 dominates, while top-fcc and top-hcp domains represent a minor contribution so that their presence
36 hardly affects our conclusions. CO intercalation detaches the layer giving rise to two further graphene
37 species, labelled as weakly and detached graphene in ref. [10]. The shape of the graphene components
38 (Lorentian width=0.23 eV, Gaussian width =0.36 eV, Asymmetry= 0.1- 0.16) was determined from
39 the spectra recorded immediately after graphene growth, where only graphene and Ni₂C are present.
40 It was kept fixed for the analysis of all other spectra.
41
42
43
44
45
46
47
48
49
50

51 Further peaks in the C1s region are due to Ni₂C, CO and CO₂.
52
53

54 CO contributes both to the C1s and to the O1s regions. Following literature [10], we considered CO
55 components corresponding to intercalated CO at top and bridge sites, to weakly adsorbed CO at atop
56 positions on graphene and to CO at bridge sites on Ni₂C; the C1s and O1s binding energies and
57 desorption temperatures are known for these species. CO at atop sites on Ni₂C was neglected since
58
59
60
61
62
63
64
65

1
2
3
4
5
6
7
8
9
10
11
12
13
14
15
16
17
18
19
20
21
22
23
24
25
26
27
28
29
30
31
32
33
34
35
36
37
38
39
40
41
42
43
44
45
46
47
48
49
50
51
52
53
54
55
56
57
58
59
60
61
62
63
64
65

its intensity is negligible due to its lower saturation coverage and the extension of the Ni₂C covered areas in our experiment. The width of the O1s components related to CO adsorbed species was taken to be the same and fixed to the value determined for CO on bare Ni(111) (Lorentzian width=0.89 eV; Gaussian width=1.00 eV).

Finally, under NAPXPS conditions, gas-phase CO is observed as well. Its apparent E_b depends on the work function of the sample and allows therefore to determine its change. In accord with the literature [10,17], the width of the O1s peak is larger than the one of the C1s peak. The latter has non-negligible contributions due to the excitation of the internal stretch mode and of its overtones.

Under UHV conditions, the ratio of the O 1s and C 1s peak areas of CO is determined by the corresponding photoemission cross-sections ($\sigma_{C1s}=1.5$ Mb; $\sigma_{O1s}=3.5$ Mb at 650 eV), the transmission function of the analyser being constant over the scanned energy interval.

As in our previous paper [13], in order to fit the O 1s and C 1s regions self-consistently, we firstly determined the intensity of the different O 1s components and fitted the C 1s region eventually by imposing that the C 1s intensity of each adsorbed species, $I_{C1s\ ads}$, satisfies the relationship:

$$I_{O1s\ ads}/I_{O1s\ CO\ gas} = \varepsilon I_{C1s\ ads}/I_{C1s\ CO\ gas} \quad (3)$$

Where ε is the stoichiometry ($\varepsilon=1$ for CO and $\varepsilon=2$ for CO₂), $I_{O1s\ ads}$ is the intensity of the O 1s line of the adsorbed moiety and $I_{O1s\ gas}$ and $I_{C1s\ gas}$ are the intensities of the corresponding gas-phase CO lines.

The photoemission signal in NAPXPS conditions is attenuated due to scattering off gas-phase molecules. Such attenuation depends on the gas density between the sample and the entrance slit to the analyser, on their distance and on the kinetic energy of scattered photoelectrons. During CO intercalation, the sample temperature is varied from 300 K to 550 K, thus modifying the gas density above the sample. The perfect gas law may be applied in the reasonable assumption that, close to the sample where the XPS signal of gas-phase CO is collected, the latter is thermalised at the sample temperature. Despite that, the quantitative correction of the attenuation of the photoemission signal remains somewhat arbitrary: indeed, normalisation with respect to the background intensity, as performed under UHV conditions, is meaningless because also background electrons are affected by scattering off gas-phase molecules.

The following systematic errors may further influence the ratio of the O 1s and C 1s intensities :

a) photoelectron diffraction for the signal of adsorbed species;

1
2 b) a different attenuation of the photoemission signal for adsorbed and gas-phase molecules since the
3 latter are closer to the nozzle so that their photoemission signal is transmitted to the analyser through
4 a shorter path.

5
6 c) uncontrolled changes in the position of the sample during annealing and cooling procedures, which
7 may modify the distance between the collimator and the sample.
8

9
10 These effects are difficult to estimate. In the present analysis, we neglect them since they may affect
11 the absolute value of the estimated surface coverage but not the general conclusions of the manuscript.
12

13
14 To *estimate* the coverage of the different species, we assume that the surface is initially entirely
15 covered by graphene and carbide. This assumption is undoubtedly true before CO exposure, when no
16 CO-related signal is observed in the O 1s region (Fig. 2, bottom-right spectrum); indeed, if bare
17 Ni(111) patches were present, they would be rapidly covered by the residual CO molecules present
18 in the gas phase even in UHV conditions. Since a full monolayer (ML) of G and of Ni₂C corresponds
19 to 2 ML and 0.5 ML of C (in ML of Ni(111)), respectively, the fraction of surface area covered by
20 graphene (f_G) and by carbide (f_{Carb}) can be obtained from the intensities I_G and I_{Carb} of the
21 corresponding C 1s lines as follows:
22

$$23 \quad f_G = \frac{I_G}{I_G + 4 I_{\text{Carb}}} \quad \text{and} \quad f_{\text{Carb}} = 1 - f_G.$$

24
25 The G and Ni₂C coverages (θ_G and θ_{Carb} , respectively) are thus given by $\theta_G = 2 f_G$ and $\theta_{\text{Carb}} = \frac{1}{2} f_{\text{Carb}}$.
26 The coverage of CO and CO₂ is then determined by comparing the corresponding C 1s intensity to
27 the one of the graphene recorded at the same pressure and temperature. Since such species are
28 intercalated, the so-obtained coverage must be further corrected for the attenuation factor of the
29 photoemitted electron yield by the graphene layer ($f_{\text{att}} \sim 2.3$, as determined in ref. [18]). However,
30 some uncertainty remains for lines that cannot be separated, e.g. those corresponding to intercalated
31 CO bonded at atop Ni(111) sites and weakly bonded CO adsorbed at atop graphene sites. A reasonable
32 procedure to disentangle these contributions will be discussed in the following.
33

34
35 Under NAP conditions, photoemission peaks due to the gas-phase species also enables tracking of
36 the work function changes of the sample ($\Delta\phi$) by comparing the apparent E_b shifts of such species.
37 Indeed, the change in the binding energy of the Fermi Level $\Delta(E_{b \text{ FL}})$ is proportional to $-\Delta\phi$ by:
38

$$39 \quad \Delta\phi = -K \cdot \Delta(E_{b \text{ FL}} (\text{gas- phase})) \quad (4)$$

1
2
3
4
5
6
7
8
9
10
11
12
13
14
15
16
17
18
19
20
21
22
23
24
25
26
27
28
29
30
31
32
33
34
35
36
37
38
39
40
41
42
43
44
45
46
47
48
49
50
51
52
53
54
55
56
57
58
59
60
61
62
63
64
65

with K being a constant close to unity [19]. This relationship holds because the E_b of the gas-phase species is plotted with respect to the Fermi edge of the sample and the inspected gas-phase molecules are at the same potential as the surface due to the focal properties of the analyser

3. Results and discussion.

Fig. 2 shows sample spectra of the C 1s (left panel) and O 1s (right panel) regions recorded before and during exposure of the graphene-covered Ni(111) to CO. The pressure is set at 3.7 mbar and decreased by less than 10% during the experiment. Table 1 summarises the binding energies of the different components emerging from the fitting procedure with their assignment.

It is apparent that:

- a) Before introducing CO into the experimental chamber, oxygen is present only in trace amounts on the sample (at most 0.02 ML, see spectrum I-right). The corresponding C 1s region shows features at 284.7 eV and 283.4 eV, related mainly to strongly interacting graphene and Ni₂C, respectively, with only a minor contribution at 284.3 eV due to weakly interacting graphene.
- b) Spectra II to V are significantly modified by introducing 3.7 mbar of CO into the experimental chamber since peaks due to gas-phase CO appear in O 1s and C 1s regions around 537.9 eV and 291.3 eV, respectively. The binding energies of these peaks change during the experiment due to the variation of the work function of the sample. The asymmetric shape of the C 1s feature (see insets in Fig. 2-left) is due to the presence of vibrational overtones.
- c) Upon introduction of CO, a broad structure, due to the convolution of new peaks at 531.0 eV, 531.4 eV and 532.2 eV, forms in the O 1s region already at 320 K (spectrum II). Also, the shape of the corresponding C 1s spectrum changes and can be deconvolved into components corresponding to different types of graphene and CO at different adsorption sites (see table I). Following refs. [10,13], we assign the O 1s lines at 531.0 eV and 531.4 eV to bridge-bonded CO intercalated under the graphene layer and to CO at Ni₂C patches, respectively. The corresponding C 1s lines at 285.4 eV and 285.8 eV overlap with the tail of the intense graphene features. The O 1s component at 532.2 eV and its companion at 286.0 eV are identified with atop CO. The alternative assignment of the 532.2 eV peak to OH contamination is ruled out since it should be coupled to the presence of water molecules in the gas-phase. However, no gas-phase H₂O signal is detected at $E_b(\text{O } 1s)=536.0$ eV [20] in the NAPXPS spectrum. Indeed the intensity at that binding energy is less than 1% of that of

1 gas-phase CO. Water intercalation followed by dissociation is not possible at such low partial
2 pressures. The C 1s components at 283.9 eV and at 284.3 eV are due to detached and weakly
3 interacting graphene, respectively [10,21]
4

- 5 d) Upon annealing above 340 K (spectrum III), weakly interacting graphene becomes dominant
6 over the strongly interacting one; also, the detached graphene component increases in
7 intensity.
8
9
10 e) Finally, a new feature grows at 533.4 eV and becomes prominent over the other O 1s
11 components for $T \geq 425$ K (spectra IV and V). This species is accompanied by the appearance
12 of a C 1s line at 291.3 eV, which partly overlaps with the signal due to gas-phase CO. We
13 assign it to physisorbed CO₂ [13]. Given its low adsorption energy, it must be trapped under
14 the graphene cover in order not to desorb at the temperature of the present experiment. We
15 suggest that it is produced by the Boudouard reaction.
16
17
18
19
20
21
22
23
24
25
26
27
28
29
30
31
32
33
34
35
36
37
38
39
40
41
42
43
44
45
46
47
48
49
50
51
52
53
54
55
56
57
58
59
60
61
62
63
64
65

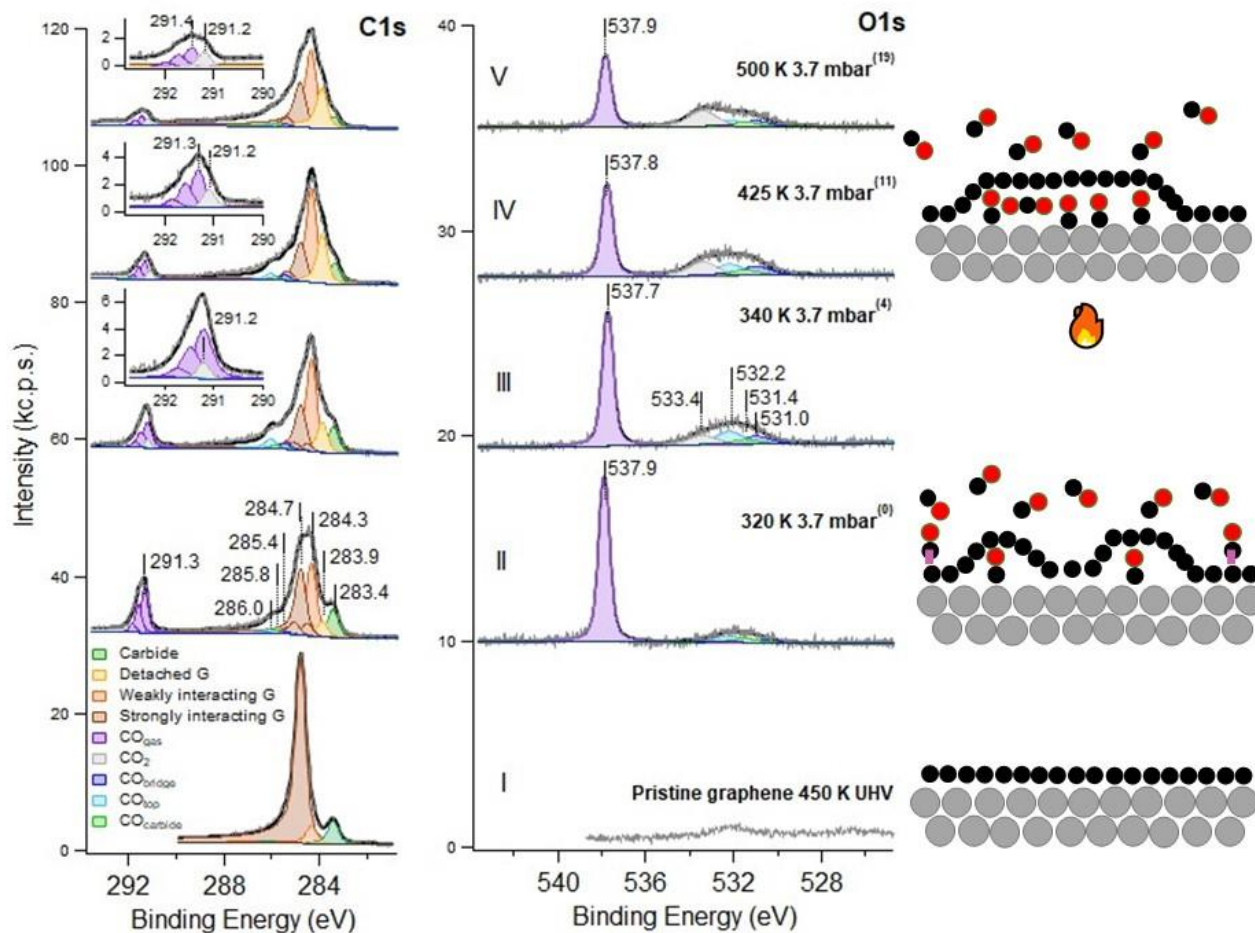


Fig. 2 NAPXPS spectra of the C 1s (left) and O 1s (right) regions for G/Ni(111) in UHV (bottom spectra) and under $P_{\text{CO}} \sim 3.7$ mbar and increasing T . $h\nu = 650$ eV for all spectra except I-left, for which $h\nu = 400$ eV. The spectra are presented without normalisation and upshifted for the sake of clarity. Note the different scales in the two panels. All the components contributing to strongly interacting graphene (top-fcc, top-bridge and the minor contribution of top-hcp) are evidenced by brown filling. The small signal present around 532 eV before intercalation is most likely due to traces of OH. Note that the photoemission intensity is strongly attenuated after filling the chamber with CO so that the intensities recorded in UHV and in the presence of gas-phase CO cannot be directly compared. The small number in each caption of the left panel indicates the corresponding point of the sequence in Fig. 3. Drawings on the right side schematise the different phases of the experiment. The purple rectangles indicate the weak bond of CO adsorbed at strongly interacting graphene areas.

Adsorbed/absorbed species	C 1s B.E. (eV)	O 1s B.E. eV)
Nickel carbide (Ni ₂ C)	283.4	-
Detached graphene	283.9	-
Weakly interacting graphene	284.3	-
Strongly interacting graphene		
bridge-top	284.7	-
top-fcc	284.5 ; 285.0	
top-hcp	285.3	
CO bridge	285.4	531.0
CO top	286.0	532.2
CO bridge on Ni ₂ C	285.8	531.4
Physisorbed CO ₂ under G	291.2	533.4

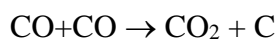
Table I. C 1s and O 1s Binding energies of the different adsorbed species and their assignment, according to refs. [13,16]

The analysis of the data presented in Fig. 2 was performed for all spectra of the series. The outcome is summarised in Fig. 3 vs spectrum number and discussed in the following. The spectra were recorded subsequently at nearly constant CO pressure (~3.7 mbar) while increasing the crystal temperature (see panel E). Panel A shows the evolution of the graphene, carbide and total carbon coverage, while panel B reports the fractional area of the different graphene species and of carbide. Panel C shows the CO and CO₂ coverage obtained, assuming that all the molecules are intercalated underneath graphene. This is not perfectly correct since the atop CO intensity results from the unresolved contributions of intercalated CO at Ni sites and of weakly bonded CO adsorbed at graphene sites, which is not screened by the graphene layer. Since the coverage is corrected for the attenuation of the G cover (roughly a factor of 2.3) for all species, the amount of weakly adsorbed CO on graphene reported in the figure is overestimated by the same factor.

Lastly, the work function change is reported in panel D. We mention that the determination of ϕ for G/Ni(111) is still controversial; values reported in the literature differ significantly, ranging from 3.66 eV [22] to 4.25 eV [23], lower than the one of 4.48 eV measured for free-standing graphene [22]. In our experiment, ϕ increases up to spectrum 7 and slowly decreases afterwards. This behaviour results from the combined effects of the graphene detachment due to CO intercalation and of the presence of weakly adsorbed CO above graphene, as discussed in the following.

1 We note that the surface fraction covered by strongly interacting graphene ($E_b=284.7$ eV) decreases
2 already from the first spectra and only partially recovers at the highest temperature (panel B).
3 Correspondingly, the weakly interacting ($E_b=284.3$ eV) and detached ($E_b=283.9$ eV) graphene areas
4 initially increase and then remain stable. In literature [1,10], the carbon-containing species with
5 $E_b(\text{C1s})\sim 284.4$ eV is ascribed to weakly interacting graphene. Africh et al. identified this phase with
6 rotated graphene domains sitting above carbide-covered areas [1]; alternatively, it might correspond
7 to the second layer of bilayer graphene patches. Neither explanation seems appropriate to describe
8 the current results: weakly interacting G cannot sit above carbide since the amount of carbide is very
9 small or even missing after G growth by C_2H_4 dehydrogenation. Moreover, weakly interacting G
10 appears promptly upon CO intercalation and grows with the detached graphene component
11 ($E_b(\text{C1s})=283.9$ eV), while carbide coverage decreases. The assignment to a second graphene layer
12 is also problematic since, in this case, the intensity of the strongly interacting G component should
13 remain more or less constant, contrary to our experimental evidence. We thus suggest that CO
14 intercalation proceeds from the edges of graphene flakes and reaction occurs far away from the
15 borders, causing the formation of graphene bubbles in which detached graphene is at the centre and
16 weakly interacting graphene (having an intermediate E_b value between those of detached and strongly
17 interacting graphene) is at the borders.

18 The total carbon coverage increases by about 0.25 ML (see Fig. 3A) with increasing temperature due
19 to the growth of the fractional area covered by graphene at the expense of the one covered by carbide.
20 The carbide carbon content (estimated as ~ 0.09 ML) is insufficient to account for this change.
21 However, the formation of CO_2 , occurring already at 340 K (panel C), is indicative of the onset of
22 the Boudouard reaction:



23 which also provides additional carbon. The estimated amount of CO_2 (~ 0.05 ML) can thus justify at
24 least part of it. We note that it is not possible to have a more precise agreement due to the difficulties
25 in the absolute coverage calibration of the adsorbed species; on the other side, the observed CO_2
26 signal might correspond to the equilibrium coverage between CO_2 production and deintercalation.
27 The carbon production by the Boudouard reaction could thus be underestimated. This hypothesis is
28 supported by the fact that the CO_2 signal promptly decreases when the chamber is evacuated (see Fig.
29 7).

30 According to literature, the E_b value of gas-phase CO_2 is expected at ~ 537 eV and 293.6 eV in the O
31 1s and C 1s regions, respectively [24,25]. Indeed, a small signal at this binding energy is sometimes

1 present in the C 1s region (not shown), but the corresponding O 1s peak never emerges in XPS spectra.
2 Since the noise level in the O 1s region is typically 4% of the O 1s intensity of gas-phase CO (at
3 $P_{\text{CO}} \sim 3.7$ mbar), we conclude that the partial pressure of gas-phase CO₂ cannot exceed 0.15 mbar,
4 implying that the Boudouard reaction rate is lower than 4% in our conditions. However, such
5 reactivity is sufficient to generate the detected coverage of physisorbed CO₂ under the graphene cover
6 and to provide the required amount of carbon.
7
8
9

10
11 The Boudouard reaction mechanism implies dissociation of CO and fast removal of the so obtained
12 O atom by another CO molecule [26]. The rate-limiting step is indeed the dissociation of CO, for
13 which process an activation barrier of about 1.5 eV was estimated theoretically [27]. UHV
14 experiments reported a much lower apparent activation energy of (0.13 ± 0.07) eV/molecule for the
15 Boudouard reaction on Ni(111) [28]. At the same time, Fowles et al. estimated an activation barrier
16 of 1.1 eV/molecule for the rate-limiting step by the carbon formation rate on a commercial catalyst
17 (and at a pressure higher than in the present study) [29]. Whatever its actual value, the reaction barrier
18 must be lowered under graphene cover due to the decrease of the CO adsorption energy. According
19 to recent DFT calculations, such quantity varies from -2.24 eV/molecule on bare Ni(111) to -0.34
20 eV/molecule under the G cover for a CO coverage of 0.14 ML, while at 0.5 ML the reduction goes
21 from -2.26 eV/molecule to -1.78 eV/molecule [2]. These arguments prove that the occurrence of the
22 Boudouard reaction under graphene cover is more likely than without it, thus supporting our
23 experimental evidence.
24
25
26
27
28
29
30
31
32
33
34
35

36 We also mention that possible alternative C sources, e.g. the occurrence of CO dissociation or C
37 segregation from the bulk, can safely be excluded. First of all, the absence of atomic oxygen (expected
38 at ~ 529.7 eV [17]) or nickel oxide (expected at ~ 530.3 eV [17]) signals in the O 1s spectrum rules
39 out that the additional carbon is generated by CO dissociation at defects. Indeed, given the high CO
40 pressure, the oxygen released by such a process could be efficiently removed by reaction with further
41 CO. Still, CO oxidation on Ni(111) occurs only at high atomic oxygen coverage while it is
42 endothermic at low oxygen coverage [30]. At 1/3 ML, the reaction has an activation barrier of 0.83
43 eV [31], while low-temperature oxidation is possible in the presence of weakly bonded atomic
44 oxygen. Also, segregation from the bulk is excluded since the G growth by this mechanism does not
45 take place below 580 K (see discussion of Fig. 1). We can thus safely conclude that the formation of
46 the additional carbon is due to the Boudouard reaction.
47
48
49
50
51
52
53
54
55
56
57
58
59
60
61
62
63
64
65

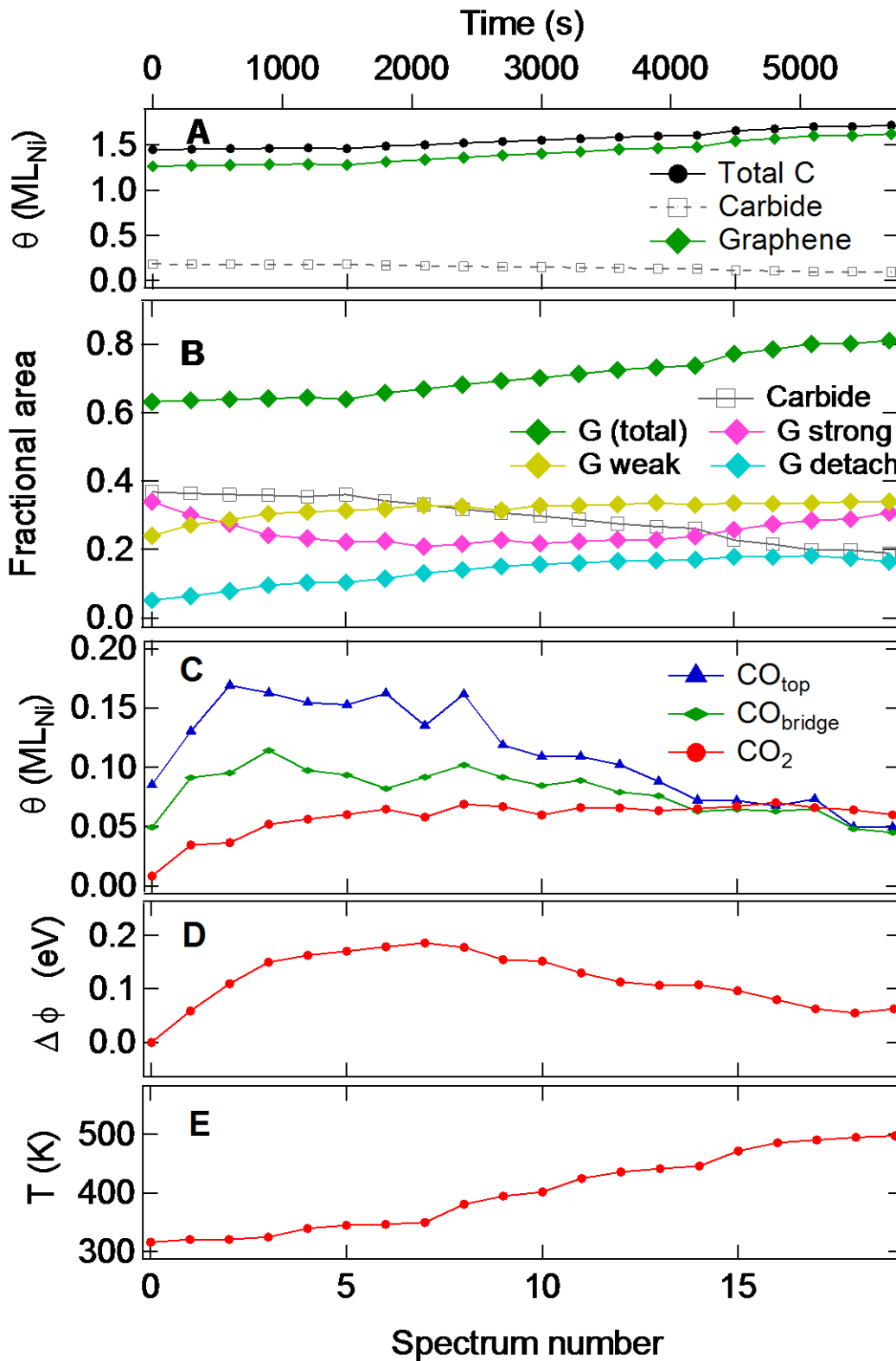


Fig. 3. Analysis of the data reported in Fig. 2. The abscissa refers to the number of subsequent spectra recorded in the experimental run. A) Graphene, carbide and total carbon coverage. B) Fractional area of the different graphene species and carbide. The procedure used to calculate these values (explained in the experimental section) assumes that the surface is entirely covered by graphene or carbide. C)

Coverage of atop- and bridge-bonded CO and of CO₂. D) Variation of the average work function. E) Sample temperature.

Fig. 3C shows that the coverage of CO molecules adsorbed both at top and bridge sites (CO_{top} and CO_{bridge}, respectively) increases rapidly upon CO exposure and decreases eventually with rising temperature. CO_{top} is initially more abundant, but at the highest T, the coverage of the two species becomes comparable. On the contrary, the CO coverage increases when the sample is cooled to 320 K, under which conditions the atop species dominates over the bridge one (see Fig. 6).

To explain this complex behaviour, we recall that both intercalated CO adsorbed at Ni(111) top sites and on-surface CO adsorbed at G top sites contribute to the 286.0 eV component. They cannot be directly resolved in the XPS spectra, but they are characterised by different thermal stability. To estimate the different contributions to the CO_{top} coverage of intercalated and on-surface CO, we start considering the equilibrium coverage (Θ) vs T for CO adsorbed on bare Ni(111) (Fig. 4, black curve) and on G/Ni(111) (purple curve) at a CO pressure of 3 mbar. Θ is obtained by equating the desorption and the adsorption rates (see Supporting online material), including the coverage dependence of the adsorption energy to improve the accuracy of the estimate. The theoretical curve for the equilibrium coverage of CO on Ni(111) is then calculated from calorimetric data [32] using a parabolic interpolation for $E_{\text{des}}^{\text{bare Ni}}(\Theta)$. For weakly adsorbed CO on G/Ni(111), a linear dependence was assumed for the desorption energy for $E_{\text{des}}^{\text{COweak}}(\Theta)$ with the initial value and the slope estimated in ref. [33]. It is apparent that desorption of weakly adsorbed CO on graphene must occur at a much lower temperature than deintercalation of CO bound to Ni(111). The decrease of the CO_{top} intensity observed in Fig. 3C must then arise mainly from the desorption of the weakly adsorbed moiety.

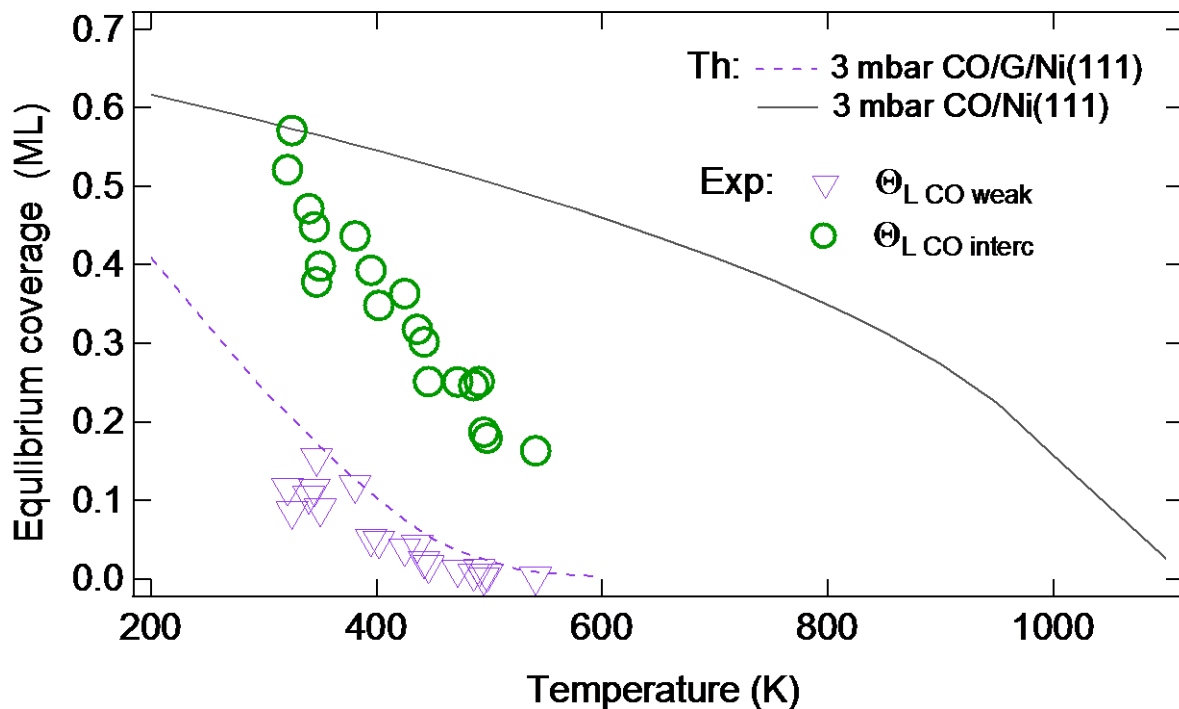


Fig. 4 Estimated equilibrium coverage of CO on Ni(111) (using the calorimetric data of ref. [32] – black curve) and for weakly adsorbed CO on G/Ni(111) (purple dashed curve - [33]). They are compared with the *local* CO coverage observed for the weakly bonded (CO_{weak}) species on graphene and the intercalated ($\text{CO}_{\text{interc}}$) one.

The variations of ϕ during the experiment (Fig. 3D) support this conclusion. In fact, its initial increase can be explained both by the adsorption of CO on graphene and by the detachment of graphene due to CO intercalation. Both effects induce a change of the same sign. On the contrary, the slow decrease observed after scan 7 is unexpected considering that, the relative amount of weakly and detached graphene increases in this temperature range, and the one of strongly interacting graphene is about constant. Therefore, the observed behaviour can be rationalised only by the desorption of weakly adsorbed CO *above* graphene.

At 500 K, only intercalated CO is stable. In this condition, we observe a comparable signal for atop and bridge bonded CO. This result is at variance with literature for the same system [2,10] and for CO on bare Ni(111) [12], for which $\text{CO}_{\text{bridge}}$ is dominant. However, on bare Ni(111), a comparable population of CO at top and bridge sites was reported by Infrared Reflection Absorption Spectroscopy for the compressed 0.57 ML phase obtained in UHV at 80 K [34]. On the contrary, little or no CO at top sites is detected experimentally for G/Ni(111) [2,10], and *ab-initio* calculations [2] predict that this species is not stable under cover. At variance with the cited papers, our experiments were

performed in-operando conditions, i.e. recording the XPS spectra in CO pressure and for $RT \leq T \leq 500$ K. Having already ruled out the possibility that the 532.2 eV signal is related to OH species, we tentatively explain the different outcome of our study with the different experimental conditions. We also mention that theoretical calculations in ref. [2] were performed for a fully detached graphene layer while, in our experiment, a mixed layer consisting of patches of strongly interacting, weakly interacting and detached graphene is present. Therefore, the situation is more complex since the coverage of intercalated CO is not uniform on the surface and areas of high local coverage of intercalated CO coexist with areas where no intercalation takes place, and CO weakly adsorbs at RT under NAP conditions. We suggest, therefore, that the total energy of such a mixed layer can be lower than the one of a fully detached layer with only bridge-bonded CO. Indeed, at high local coverage, the adsorption energy of CO under G is calculated to be around -1.7 eV/molecule, to be compared to -2.1 eV/eV molecule on bare Ni [2]. The difference, which accounts for the energy cost of detaching the graphene layer, is indeed comparable with the adsorption energy of weakly adsorbed CO above graphene, estimated experimentally to be around 0.35 eV/molecule at 1/3 ML coverage and even higher at lower coverage [33]. This explains why, despite the higher pressure with respect to previous studies [2,10], we do not observe complete delamination of the graphene layer. We speculate that in such a mixed layer, also atop CO can be stable under graphene bubbles given the high local coverage. Considering that intercalated CO is present only under detached or weakly interacting graphene areas, which cover about half of the sample, we estimate a local CO coverage of ~ 0.5 ML around RT (though it may be different under the weakly and detached G areas). Such high local coverage may allow populating of a compressed phase in which both top and bridge sites are occupied in comparable amounts under dynamical equilibrium conditions, as in the case of bare Ni(111) at low temperature and in UHV [34].

To determine the fraction of non-intercalated atop CO, we assumed that the coverage of atop and bridge CO under cover are comparable at any T, as is indeed the case at high temperatures. The total coverage of intercalated CO (Θ_{COinterc}) is then twice the one of bridge CO. The coverage of CO weakly adsorbed on graphene (Θ_{COweak}) and overlapping with intercalated CO at atop sites can then be estimated by the difference between the intensity of atop and bridge bonded CO after removing the correction for the attenuation factor $f_{\text{att}} \sim 2.3$ due to graphene, which should be applied only to the intercalated species. Since CO binds only to strongly interacting graphene [33], the *local* coverage of CO_{weak} ($\Theta_{\text{L COweak}}$) can be obtained by dividing Θ_{COweak} by the fractional area occupied by strongly interacting graphene. The resulting coverage is shown by the violet triangles in Fig. 4, which are indeed in good agreement with the expected equilibrium $\Theta_{\text{L COweak}}$. Similarly, the *local* coverage of

1
2
3
4
5
6
7
8
9
10
intercalated CO ($\Theta_{L\ COinterc}$) may be estimated by dividing $\Theta_{COinterc}$ by the total fractional area
occupied by weakly adsorbed plus detached graphene (circles in Fig. 4). It is apparent that $\Theta_{L\ COinterc}$
decreases with temperature more rapidly than expected for CO/Ni(111). This high
desorption/deintercalation rate could indicate partial conversion into CO₂ and/or lower adsorption
energy under cover. Indeed, for the similar system CO/Pt(111), the latter quantity decreases from
1.74 eV/molecule to 1.21 eV/molecule when CO is intercalated under G/Pt(111) [6].

11
12
13
14
15
16
17
18
19
Note that if the amount of intercalated atop CO were smaller, the relative amount of weakly adsorbed
CO would be even higher. A constraint on the maximum amount of weakly adsorbed CO is provided
by the intensity of the 532.2 eV remaining after the evacuation of the chamber (see Fig. 7 below),
which can only be due to intercalated CO at atop sites.

20
21
22
23
24
25
26
27
28
29
30
31
32
33
34
35
36
37
38
39
40
41
42
43
44
45
46
47
48
49
50
51
52
53
54
55
56
57
58
59
60
61
62
63
64
65
Further identification of weakly bonded CO on G/Ni(111) is provided by the experiment reported in
Fig. 5. Starting from a G/Ni(111) sample with intercalated CO, we slowly decreased the temperature
from 490 K to 313 K at nearly constant CO pressure. Upon cooling, the O 1s features related to
adsorbed species increase in intensity while the main C 1s peak decreases and a shoulder grows on
its high energy side. Both the C 1s and O 1s peaks related to gas-phase CO downshift with cooling,
indicating an increase in work function. Considering that, the relative amount of strongly interacting,
weakly interacting and detached graphene remains nearly constant in this T range, the work function
variation can only be induced by CO adsorption at G/Ni(111). Since this is the only change in the
system, it must also be responsible for the enhanced asymmetry of the C 1s line of graphene.

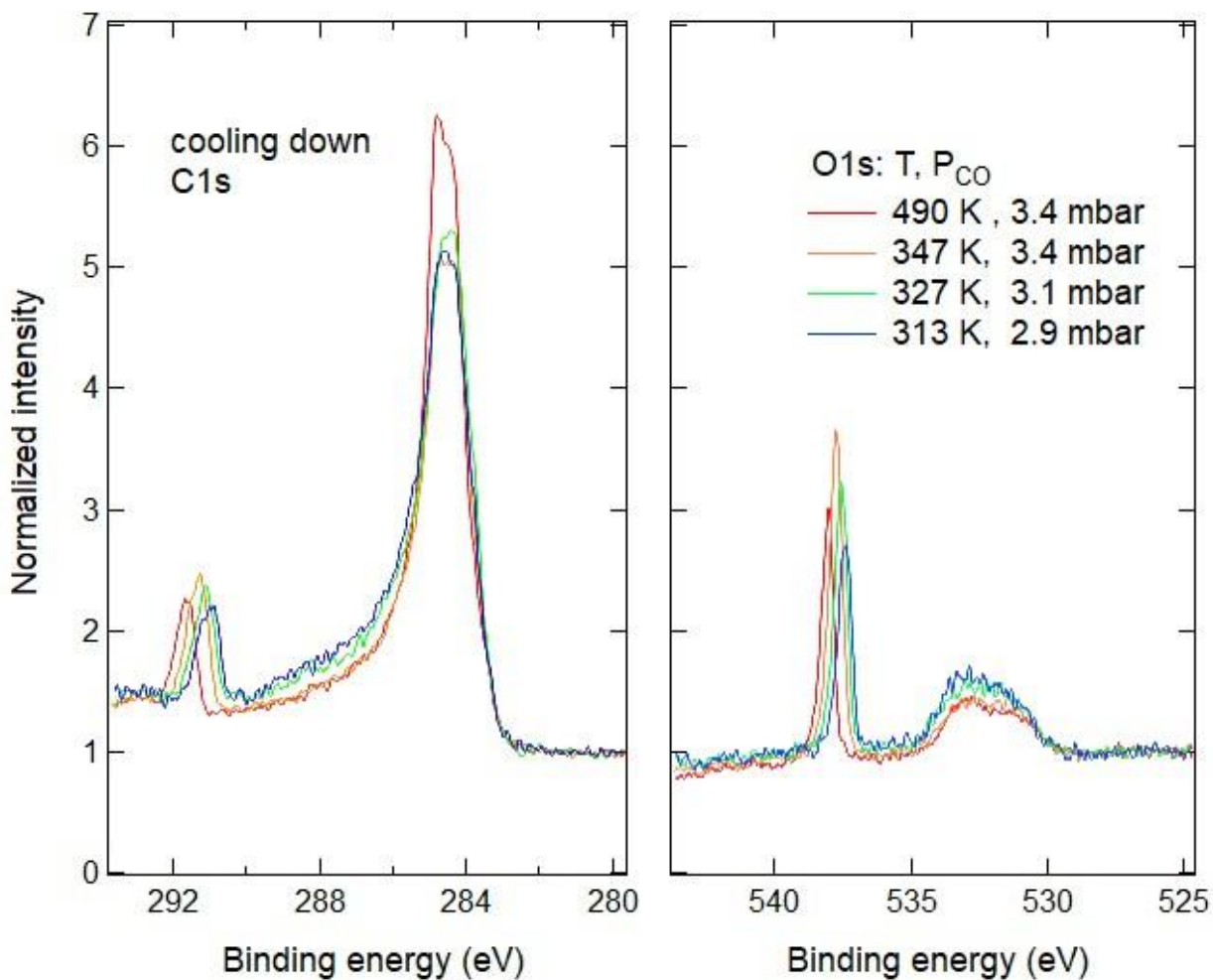


Fig. 5. C 1s (left) and O 1s (right) XPS spectra recorded while cooling the sample from 490 K to 313 K in P_{CO} ~3.1 mbar. The C 1s and O1s spectra are normalized scaling the value of the background in the low binding energy region to 1. The same data are fitted in Fig. S1 without normalization.

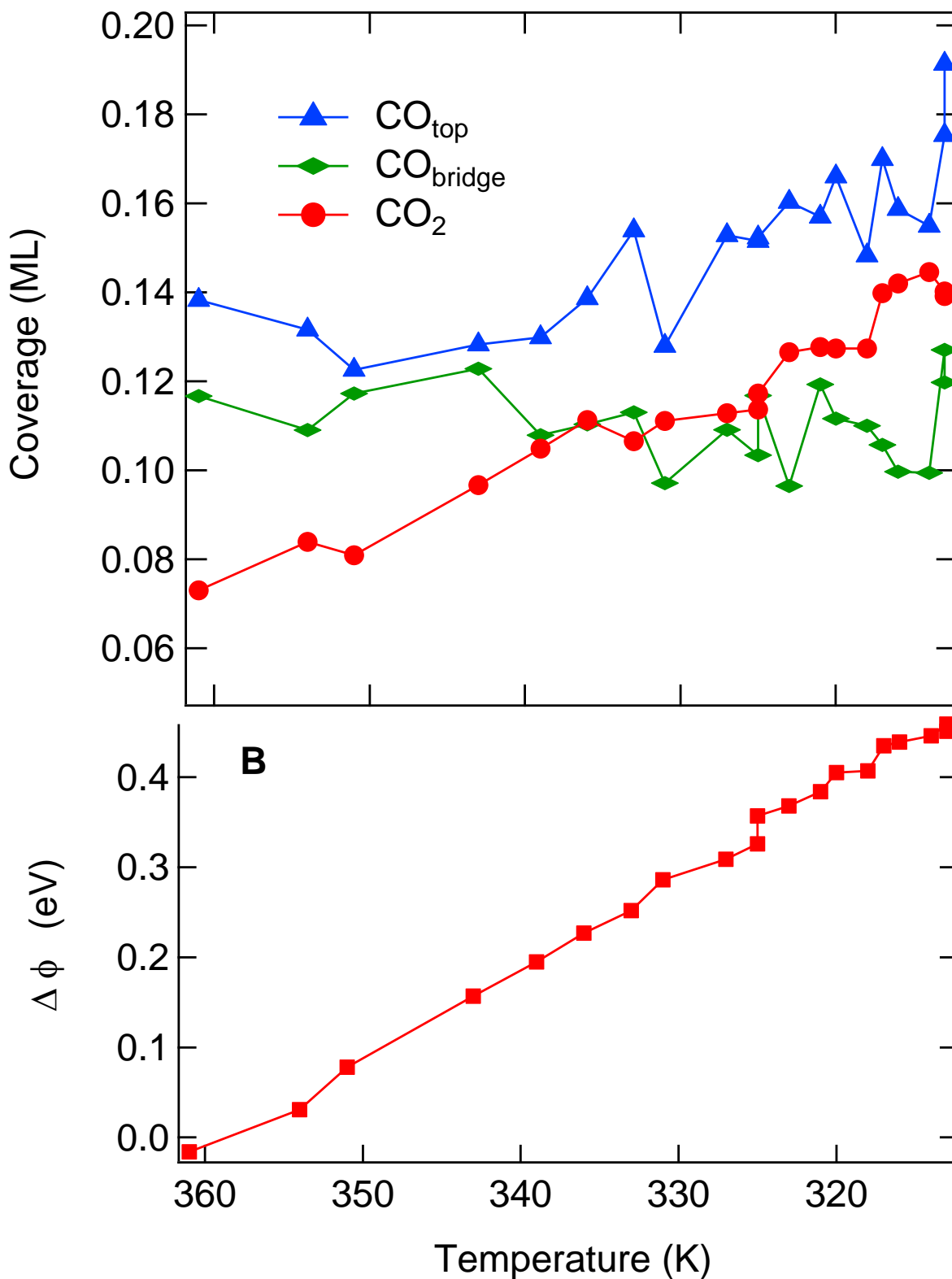


Fig. 6 Analysis of the whole sequence of spectra of the experiment in Fig. 5. A, in which the sample was cooled down in a constant CO pressure $P_{\text{CO}} \sim 3.1$ mbar. A): Coverage of $\text{CO}_{\text{bridge}}$ (green lozenges), CO_{top} (blue triangles) and CO_2 (red circles) vs T. B) Work function variation vs T. Note the reversed scale of the X-axis, corresponding to the cooling process.

1
2 In Fig. 6, the coverage of the different CO species is deduced from fitting the O 1s region (see Fig.
3 S1) and the work function change $\Delta\phi$ are plotted vs sample temperature. The CO_{top} coverage increases
4 for $T < 340$ K, while $\text{CO}_{\text{bridge}}$ remains nearly constant over the whole T range. In addition, the amount
5 of physisorbed CO_2 present under cover, corresponding to the O 1s component at 533.4 eV, grows
6 almost linearly with decreasing T. This is in apparent contradiction with the increase of the CO_2 signal
7 observed when heating the sample. The overall picture can be rationalised by reminding that CO_2
8 formation needs a considerable amount of intercalated CO, which is only present after the detachment
9 of a significant fraction of the graphene layer. Therefore, in the annealing sequence, the CO_2 signal
10 arises from the combination of two competing effects: the rate of the Boudouard reaction (decreasing
11 with increasing T) and the area of detached and weakly interacting graphene (larger at higher T).
12 When cooling down, on the contrary, it is uniquely determined by the increase of the equilibrium
13 constant of the Boudouard reaction since the catalytically active area (proportional to the amount of
14 detached/weakly interacting graphene) remains constant.

15
16 Finally, we remark that the 533.4 eV line can only be due to physisorbed CO_2 under cover. Indeed,
17 the alternative identification with transient water contamination has already been ruled out since,
18 given its low adsorption energy, a significant partial pressure of H_2O in the gas-phase would be
19 needed to justify a metastable coverage resulting in such intensity. In this case, the O 1s line of gas-
20 phase H_2O should be visible at ~ 536 eV [20], contrary to experimental evidence. We also exclude
21 that the 533.4 eV peak is due to the formation of tetracarbonyl-nickel since the corresponding feature
22 is missing in the Ni 2p spectrum, at least within our experimental sensitivity (see Fig. S3). Such a
23 signal would indeed be expected given the cross-section for Ni 2p at $h\nu=970$ eV and the one for O 1s
24 at $h\nu=650$ eV. Moreover, the formation of tetracarbonyl-nickel is expected to be thermodynamically
25 less favoured than the Boudouard reaction because it involves four CO molecules instead of two.

26
27 The signal at 533.4 eV disappears when the system is evacuated (see Fig. 7). A direct comparison of
28 the spectra under NAP and UHV conditions is not possible because of the already mentioned
29 attenuation of the signal due to gas-phase CO. To compare the spectra of Fig. 7, we, therefore,
30 proceeded as follows:

31
32 1) We assume that the graphene sheet is not affected by the evacuation process. This allows
33 determining the distance d between the sample and the nozzle by

$$34 \quad I(\text{P}_{\text{CO}}) = I_{\text{UHV}} \exp(-d/\lambda_{\text{C1s}})$$

1 where I_{UHV} and $I(\text{P}_{\text{CO}})$ are the intensity in the absence and in the presence of CO pressure, respectively.
2 The mean free path of C 1s electrons λ_{C1s} , is then calculated from the CO gas density and the cross-
3 section for inelastic scattering of electrons having the kinetic energy of C 1s electrons in our
4 experiment (taken from ref. [35] as the difference between the total cross-section and the elastic cross-
5 section).
6
7

8
9
10 2) A similar relationship is used to estimate the attenuation of the signal due to O 1s electrons using
11 the corresponding $\lambda_{\text{O 1s}}$ and the distance d .
12

13
14 3) The so-obtained correction factors for the C 1s and O 1s lines are used to rescale the corresponding
15 spectra after subtracting a linear background.
16
17

18 Upon evacuation of the experimental chamber (see Fig. 7 and Fig. S2), both the asymmetry in the C
19 1s region and the O 1s components due to CO_2 and weakly adsorbed CO disappear. The final intensity
20 of the 532.2 eV component is smaller than the one at 531.0 eV due to bridge bonded CO, which
21 remains almost unaffected. Such behaviour indicates that: i) intercalated $\text{CO}_{\text{bridge}}$ is stable at RT; ii)
22 since the intensity of CO_{top} and $\text{CO}_{\text{bridge}}$ are expected to be equal under CO pressure at RT, the fact
23 that the 532.2 eV component is now smaller indicates that part of the intercalated CO_{top} was
24 metastable and has now de-intercalated. This is coherent with the lower adsorption energy expected
25 for this species; iii) the narrowing of the graphene peak is thereby associated with the decrease of the
26 weakly interacting and detached components.
27
28
29
30
31
32
33
34
35
36
37
38
39
40
41
42
43
44
45
46
47
48
49
50
51
52
53
54
55
56
57
58
59
60
61
62
63
64
65

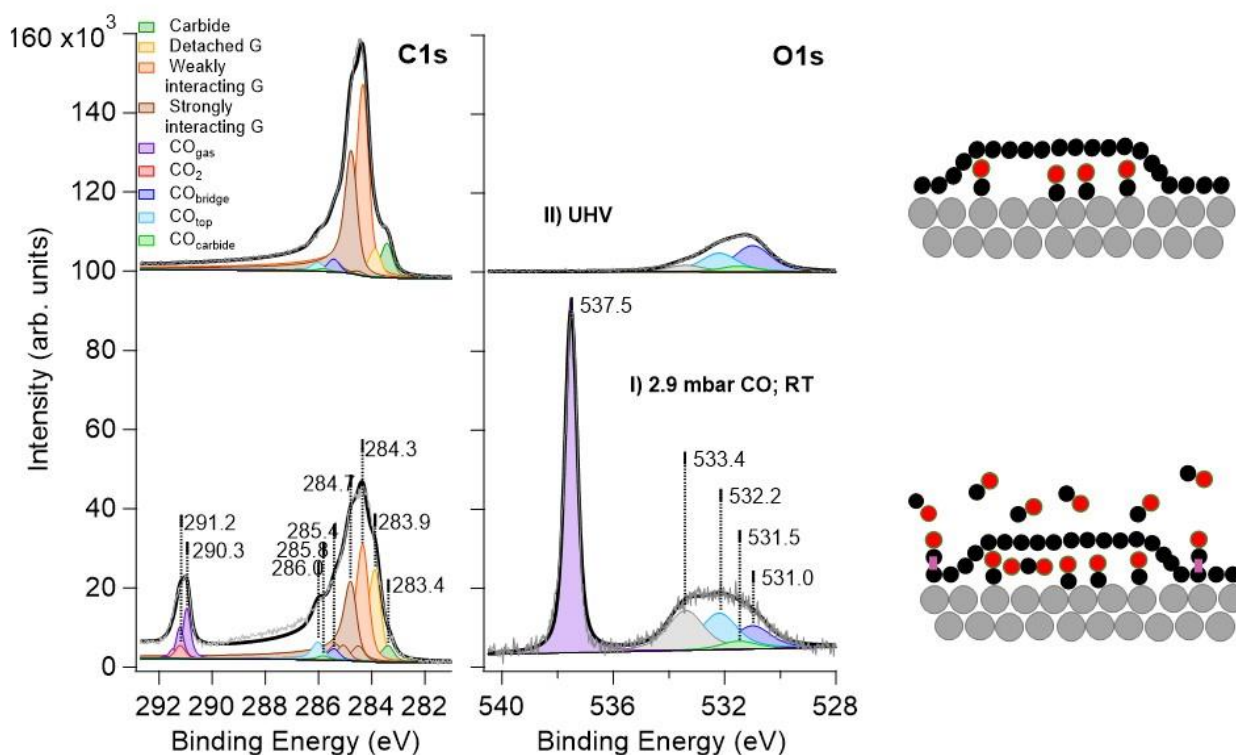


Fig. 7. Comparison of the XPS spectra of G/Ni(111) at T=313 K before (bottom, $P_{\text{CO}}=2.9$ mbar) and after (top, UHV) evacuating the experimental chamber. The spectra of the C 1s and of the O 1s region have been corrected for the attenuation due to the gas-phase (see text).

4. Conclusions

We have investigated CO intercalation under G/Ni(111) for so far unexplored in-operando NAP conditions. Our experiments show that:

- CO intercalates below graphene, binding to Ni(111) both at atop and bridge sites, indicating a local coverage of CO higher than the ones observed so far without monitoring the surface in real-time.
- This high local CO coverage enables the formation of physisorbed CO_2 under the graphene cover via the Boudouard reaction already at 340 K. Its accumulation underneath graphene is evident in the NAPXPS spectra. At the same time, the absence of the corresponding gas-phase signal indicates a small reaction probability. The generated carbon converts carbide into

1 graphene, enlarging the fraction of the graphene-covered surface. To the best of our
2 knowledge, this result is the first demonstration of the occurrence of the Boudouard reaction
3 on Ni(111) under graphene cover already close to RT. Since the reaction rate increases with
4 CO pressure, we expect this result to be relevant under catalytic conditions on nickel-based
5 catalysts involving the presence of gas-phase CO, also as a side product.
6
7

- 8
9 c) CO adsorbs above strongly interacting domains of the G layer. Such results confirm our
10 previous findings obtained in UHV at low temperature [33], from which a relevant
11 equilibrium coverage of CO at RT in the mbar pressure range was predicted. Such weakly
12 bound CO might effectively enable a higher rate for reactions involving CO, thanks to the
13 lower activation barrier.
14
15
16
17

18 These conclusions are expected to have an impact on the study of chemical reactions undercover [36]
19 and contribute to filling the pressure gap between previous NAP studies and the real catalytic
20 conditions at even higher pressures.
21
22
23
24
25
26

27 **Acknowledgements**

28
29
30
31
32 We acknowledge financial support from MIUR through projects PRIN2017 n. 2017NYPHN8 and
33 n. 2017KFMJ8E_003 and from Fondazione Compagnia di S. Paolo through project MC-nano.
34
35

36
37 G.C. and M.L. acknowledge financial support from the Foundation for Polish Science (First
38 TEAM/2016-2/14 (POIR.04.04.00-00-28CE/16-00) project co-financed by the European Union
39 under the European Regional Development Fund) and the National Science Centre of Poland
40 (OPUS 8 2014/15/B/ST3/02927 project), respectively.
41
42
43
44

45 We acknowledge the helpful discussion with Stefano Stranges, Cristiana Di Valentin and Daniele
46 Perilli. We also acknowledge Cristina Africh and Cinzia Cepek for private communications about
47 their experiment.
48
49
50
51
52

53 **References**

- 54
55
56 [1] C. Africh, C. Cepek, L.L. Patera, G. Zamborlini, P. Genoni, T.O. Montes, A. Sala, A.
57 Locatelli, G. Comelli, T.O. Montes, A. Sala, A. Locatelli, G. Comelli, Switchable graphene-
58 substrate coupling through formation/dissolution of an intercalated Ni-carbide layer, Sci.
59
60
61
62
63
64
65

Rep. 6 (2016) 1–8. <https://doi.org/10.1038/srep19734>.

- 1
2
3 [2] S. Del Puppo, V. Carnevali, D. Perilli, F. Zarabara, A.L. Rizzini, G. Fornasier, E. Zupanič, S.
4 Fiori, L.L. Patera, M. Panighel, S. Bhardwaj, Z. Zou, G. Comelli, C. Africh, C. Cepek, C. Di
5 Valentin, M. Peressi, Tuning graphene doping by carbon monoxide intercalation at the
6 Ni(111) interface, *Carbon N. Y.* 176 (2021) 253–261.
7
8 <https://doi.org/10.1016/j.carbon.2021.01.120>.
9
10
11 [3] M. Gyamfi, T. Eelbo, M. Waniowska, R. Wiesendanger, Inhomogeneous electronic
12 properties of monolayer graphene on Ru(0001), *Phys. Rev. B - Condens. Matter Mater. Phys.*
13 83 (2011) 1–4. <https://doi.org/10.1103/PhysRevB.83.153418>.
14
15
16 [4] A. Dong, Q. Fu, M. Wei, X. Bao, Graphene-metal interaction and its effect on the interface
17 stability under ambient conditions, *Appl. Surf. Sci.* 412 (2017) 262–270.
18
19 <https://doi.org/10.1016/j.apsusc.2017.03.240>.
20
21
22 [5] X. Fei, L. Zhang, W. Xiao, H. Chen, Y. Que, L. Liu, K. Yang, S. Du, H.J. Gao, Structural
23 and electronic properties of Pb- intercalated graphene on Ru(0001), *J. Phys. Chem. C.* 119
24 (2015) 9839–9844. <https://doi.org/10.1021/acs.jpcc.5b00528>.
25
26
27 [6] Y. Yao, Q. Fu, Y.Y. Zhang, X. Weng, H. Li, M. Chen, L. Jin, A. Dong, R. Mu, P. Jiang, L.
28 Liu, H. Bluhm, Z. Liu, S.B. Zhang, X. Bao, Graphene cover-promoted metal-catalyzed
29 reactions, *Proc. Natl. Acad. Sci.* 111 (2014) 17023–17028.
30
31 <https://doi.org/10.1073/pnas.1416368111>.
32
33
34 [7] Q. Fu, X. Bao, Surface chemistry and catalysis confined under two-dimensional materials,
35 *Chem. Soc. Rev.* 46 (2017) 1842–1874. <https://doi.org/10.1039/c6cs00424e>.
36
37
38 [8] L. Gao, Q. Fu, J. Li, Z. Qu, X. Bao, Enhanced CO oxidation reaction over Pt nanoparticles
39 covered with ultrathin graphitic layers, *Carbon N. Y.* 101 (2016) 324–330.
40
41 <https://doi.org/10.1016/j.carbon.2016.01.100>.
42
43
44 [9] L. Gao, Q. Fu, M. Wei, Y. Zhu, Q. Liu, E. Crumlin, Z. Liu, X. Bao, Enhanced Nickel-
45 Catalyzed Methanation Confined under Hexagonal Boron Nitride Shells, *ACS Catal.* 6
46 (2016) 6814–6822. <https://doi.org/10.1021/acscatal.6b02188>.
47
48
49 [10] M. Wei, Q. Fu, Y. Yang, W. Wei, E. Crumlin, H. Bluhm, X. Bao, Modulation of Surface
50 Chemistry of CO on Ni(111) by Surface Graphene and Carbidic Carbon, *J. Phys. Chem. C.*
51 119 (2015) 13590–13597. <https://doi.org/10.1021/acs.jpcc.5b01395>.
52
53
54
55
56
57
58
59
60
61
62
63
64
65

- 1
2
3
4
5
6
7
8
9
10
11
12
13
14
15
16
17
18
19
20
21
22
23
24
25
26
27
28
29
30
31
32
33
34
35
36
37
38
39
40
41
42
43
44
45
46
47
48
49
50
51
52
53
54
55
56
57
58
59
60
61
62
63
64
65
- [11] I.P. Prosvirin, A. V. Bukhtiyarov, H. Bluhm, V.I. Bukhtiyarov, Application of near ambient pressure gas-phase X-ray photoelectron spectroscopy to the investigation of catalytic properties of copper in methanol oxidation, *Appl. Surf. Sci.* 363 (2016) 303–309. <https://doi.org/10.1016/j.apsusc.2015.11.258>.
- [12] G. Held, J. Schuler, W. Sklarek, H.-P. Steinrück, Determination of adsorption sites of pure and coadsorbed CO on Ni(111) by high resolution X-ray photoelectron spectroscopy, *Surf. Sci.* 398 (1998) 154–171. [https://doi.org/10.1016/S0039-6028\(98\)80020-4](https://doi.org/10.1016/S0039-6028(98)80020-4).
- [13] R. Davì, G. Carraro, M. Stojkowska, M. Smerieri, L. Savio, M. Lewandowski, J.-J. Gallet, F. Bournel, M. Rocca, L. Vattuone, Graphene growth on Ni (1 1 1) by CO exposure at near ambient pressure, *Chem. Phys. Lett.* 774 (2021) 138596. <https://doi.org/10.1016/j.cplett.2021.138596>.
- [14] H. Liu, A. Zakhtser, A. Naitabdi, F. Rochet, F. Bournel, C. Salzemann, C. Petit, J.J. Gallet, W. Jie, Operando Near-Ambient Pressure X-ray Photoelectron Spectroscopy Study of the CO Oxidation Reaction on the Oxide/Metal Model Catalyst ZnO/Pt(111), *ACS Catal.* 9 (2019) 10212–10225. <https://doi.org/10.1021/acscatal.9b02883>.
- [15] E. Celasco, G. Carraro, M. Smerieri, L. Savio, M. Rocca, L. Vattuone, Influence of growing conditions on the reactivity of Ni supported graphene towards CO, *J. Chem. Phys.* 146 (2017) 104704. <https://doi.org/10.1063/1.4978234>.
- [16] W. Zhao, S.M. Kozlov, O. Höfert, K. Gotterbarm, M.P.A. Lorenz, F. Viñes, C. Papp, A. Görling, H.-P. Steinrück, Graphene on Ni(111): Coexistence of Different Surface Structures, *J. Phys. Chem. Lett.* 2 (2011) 759–764. <https://doi.org/10.1021/jz200043p>.
- [17] E. Monachino, M. Greiner, A. Knop-Gericke, R. Schlögl, C. Dri, E. Vesselli, G. Comelli, Reactivity of carbon dioxide on nickel: Role of CO in the competing interplay between oxygen and graphene, *J. Phys. Chem. Lett.* 5 (2014) 1929–1934. <https://doi.org/10.1021/jz5007675>.
- [18] J. Kraus, R. Reichelt, S. Günther, L. Gregoratti, M. Amati, M. Kiskinova, A. Yulaev, I. Vlassiuk, A. Kolmakov, Photoelectron spectroscopy of wet and gaseous samples through graphene membranes, *Nanoscale.* 6 (2014) 14394–14403. <https://doi.org/10.1039/c4nr03561e>.
- [19] S. Axnanda, M. Scheele, E. Crumlin, B. Mao, R. Chang, S. Rani, M. Faiz, S. Wang, A.P. Alivisatos, Z. Liu, Direct work function measurement by gas phase photoelectron

spectroscopy and its application on PbS nanoparticles, *Nano Lett.* 13 (2013) 6176–6182.
<https://doi.org/10.1021/nl403524a>.

- [20] D.I. Patel, D. Shah, S. Bahr, P. Dietrich, M. Meyer, A. Thißen, M.R. Linford, Water vapor, by near-ambient pressure XPS, *Surf. Sci. Spectra.* 26 (2019) 014026.
<https://doi.org/10.1116/1.5111634>.
- [21] D. Perilli, S. Fiori, M. Panighel, H. Liu, C. Cepek, M. Peressi, G. Comelli, C. Africh, C. Di Valentin, Mechanism of CO Intercalation through the Graphene/Ni(111) Interface and Effect of Doping, *J. Phys. Chem. Lett.* 11 (2020) 8887–8892.
<https://doi.org/10.1021/acs.jpcclett.0c02447>.
- [22] G. Giovannetti, P. Khomyakov, G. Brocks, V. Karpan, J. van den Brink, P. Kelly, Doping Graphene with Metal Contacts, *Phys. Rev. Lett.* 101 (2008) 026803.
<https://doi.org/10.1103/PhysRevLett.101.026803>.
- [23] E. Del Castillo, S. Achilli, S. Tognolini, E. Fava, S. Ponzoni, G. Drera, C. Cepek, L.L. Patera, C. Africh, E. Del Castillo, M.I. Trioni, S. Pagliara, Surface states characterization in the strongly interacting graphene/Ni(111) system, *New J. Phys.* 20 (2018).
<https://doi.org/10.1088/1367-2630/aae7a0>.
- [24] S. Blomberg, M.J. Hoffmann, J. Gustafson, N.M. Martin, V.R. Fernandes, A. Borg, Z. Liu, R. Chang, S. Matera, K. Reuter, E. Lundgren, In situ x-ray photoelectron spectroscopy of model catalysts: At the edge of the gap, *Phys. Rev. Lett.* 110 (2013) 1–5.
<https://doi.org/10.1103/PhysRevLett.110.117601>.
- [25] T.G. Avval, S. Chatterjee, S. Bahr, P. Dietrich, M. Meyer, A. Thißen, M.R. Linford, Carbon dioxide gas, CO₂ (g), by near-ambient pressure XPS, *Surf. Sci. Spectra.* 26 (2019) 014022.
<https://doi.org/10.1116/1.5053761>.
- [26] D. Hua, G. Li, H. Lu, X. Zhang, P. Fan, Investigation of carbon formation on Ni/YSZ anode of solid oxide fuel cell from CO disproportionation reaction, *Int. Commun. Heat Mass Transf.* 91 (2018) 23–29. <https://doi.org/10.1016/j.icheatmasstransfer.2017.11.014>.
- [27] Y. Morikawa, J.J. Mortensen, B. Hammer, J.K. Nørskov, CO adsorption and dissociation on Pt(111) and Ni(111) surfaces, *Surf. Sci.* 386 (1997) 67–72. [https://doi.org/10.1016/S0039-6028\(97\)00337-3](https://doi.org/10.1016/S0039-6028(97)00337-3).
- [28] H. Nakano, J. Nakamura, Carbide-induced reconstruction initiated at step edges on Ni(1 1 1), *Surf. Sci.* 482–485 (2001) 341–345. [https://doi.org/10.1016/S0039-6028\(00\)01014-1](https://doi.org/10.1016/S0039-6028(00)01014-1).

- 1
2
3
4
5
6
7
8
9
10
11
12
13
14
15
16
17
18
19
20
21
22
23
24
25
26
27
28
29
30
31
32
33
34
35
36
37
38
39
40
41
42
43
44
45
46
47
48
49
50
51
52
53
54
55
56
57
58
59
60
61
62
63
64
65
- [29] J.W. Snoeck, G.F. Froment, M. Fowles, Steam/CO₂ reforming of methane. Carbon filament formation by the Boudouard reaction and gasification by CO₂, by H₂, and by steam: Kinetic study, *Ind. Eng. Chem. Res.* 41 (2002) 4252–4265. <https://doi.org/10.1021/ie010666h>.
- [30] Y. Zhang, X.R. Shi, C. Sun, S. Huang, Z. Duan, P. Ma, J. Wang, CO oxidation on Ni-based single-atom alloys surfaces, *Mol. Catal.* 495 (2020) 111154. <https://doi.org/10.1016/j.mcat.2020.111154>.
- [31] G. Peng, L.R. Merte, J. Knudsen, R.T. Vang, E. Lægsgaard, F. Besenbacher, M. Mavrikakis, On the mechanism of low-temperature CO oxidation on Ni(111) and NiO(111) surfaces, *J. Phys. Chem. C.* 114 (2010) 21579–21584. <https://doi.org/10.1021/jp108475e>.
- [32] J.T. Stuckless, N. Al- Sarraf, C. Wartnaby, D.A. King, Calorimetric heats of adsorption for CO on nickel single crystal surfaces, *J. Chem. Phys.* 99 (1993) 2202–2212. <https://doi.org/10.1063/1.465282>.
- [33] M. Smerieri, E. Celasco, G. Carraro, A. Lusuan, J. Pal, G. Bracco, M. Rocca, L. Savio, L. Vattuone, Enhanced Chemical Reactivity of Pristine Graphene Interacting Strongly with a Substrate: Chemisorbed Carbon Monoxide on Graphene/Nickel(1 1 1), *ChemCatChem.* 7 (2015) 2328–2331. <https://doi.org/10.1002/cctc.201500279>.
- [34] M. Trenary, K.J. Uram, J.T. Yates, An infrared reflection-absorption study of CO chemisorbed on clean and sulfided Ni(111) — Evidence for local surface interactions, *Surf. Sci.* 157 (1985) 512–538. [https://doi.org/10.1016/0039-6028\(85\)90689-2](https://doi.org/10.1016/0039-6028(85)90689-2).
- [35] Y. Itikawa, Cross Sections for Electron Collisions With Carbon Dioxide, *J. Phys. Chem. Ref. Data.* 31 (2002) 749–767. <https://doi.org/10.1063/1.1481879>.
- [36] E.E. Santiso, M.K. Kostov, A.M. George, M.B. Nardelli, K.E. Gubbins, Confinement effects on chemical reactions—Toward an integrated rational catalyst design, *Appl. Surf. Sci.* 253 (2007) 5570–5579. <https://doi.org/10.1016/j.apsusc.2006.12.121>.

Declaration of interests

The authors declare that they have no known competing financial interests or personal relationships that could have appeared to influence the work reported in this paper.

The authors declare the following financial interests/personal relationships which may be considered as potential competing interests:

CREDIT AUTHOR STATEMENT

R.Davì performed the measurements and the analysis, prepared the figures and wrote the manuscript.

G. Carraro, M. Stojkovska, M. Smerieri performed the measurements.

M. Bournel and J. Gallet provided assistance before and during the beamtime.

M. Lewandowski contributed to the discussion.

L. Savio and M. Rocca contributed to the discussion and to the analysis of the data.

L. Vattuone performed the measurements, wrote the manuscript and coordinated the collaboration.

All authors revised the manuscript.



Click here to access/download

Supplementary Material for on-line publication only
Vattuone_SUPPORTINGMATERIAL_revision_2022_5_3
_unmarked.docx

Dear Editor,

we are glad that both referees considered our response to their comments satisfactory, except for the points raised by Reviewer n.4 regarding the labelling in Figs. 1, 2 and 5.

We accept the criticism and:

- 1) In Fig. 1 we removed "(arb. units)" from the intensity label for better consistency with Fig. 5
- 2) In Fig. 2 we corrected the scale labelling. Indeed, the factor 10^3 was missing in the O1s panel.
- 3) We revised Fig.5, normalizing the intensities on the low binding-energy side.

We thank the reviewer for pointing out these inconsistencies.

Having addressed all the (minor) comments of Reviewer 4 we are confident that the manuscript can be accepted for publication.

Best regards

Luca Vattuone

RESPONSE TO REVIEWERS

We are glad that both referees considered our response to their comments satisfactory, except for the points raised by Reviewer n.4 regarding the labelling in Figs. 1, 2 and 5.

We accept the criticism and:

- 1) In Fig. 1 we removed "(arb. units)" from the intensity label for better consistency with Fig. 5
- 2) In Fig. 2 we corrected the scale labelling. Indeed, the factor 10^3 was missing in the O1s panel.
- 3) We revised Fig.5, normalizing the intensities on the low binding-energy side.

We thank the reviewer for pointing out these inconsistencies.

Boudouard reaction under graphene cover on Ni(111)

Rocco Davì^{1,3}, Giovanni Carraro^{2,3,4}, Marija Stojkowska^{1,3}, Marco Smerieri³, Letizia Savio³, Mikołaj Lewandowski⁴, Jean-Jacques Gallet^{5,6}, Fabrice Bournel^{5,6}, Mario Rocca^{2,3} and Luca Vattuone^{2,3*}

1 DCCI, Università degli Studi di Genova, Via Dodecaneso 31, 16146 Genova (Italy)

2 DIFI, Università degli Studi di Genova, Via Dodecaneso 33, 16146 Genova (Italy)

3 IMEM-CNR, UOS di Genova, Via Dodecaneso 33, 16146 Genova (Italy)

4 NanoBioMedical Centre, Adam Mickiewicz University, Wszechnicy Piastowskiej 3, 61-614 Poznań, Poland

5 Sorbonne Université, CNRS, Laboratoire de Chimie Physique Matière et Rayonnement, UMR 7614, Campus Pierre et Marie Curie, 4 place Jussieu, 75252 Paris Cedex 05, France

6 Synchrotron SOLEIL, L'Orme des Merisiers, Saint-Aubin, F-91192 Gif-sur-Yvette, France

* Corresponding author. Tel: +39 010 353 6554 <mailto:vattuone@fisica.unige.it>

Field Code Changed

Formatted: English (United States)

Abstract

We investigated the interaction of CO with graphene/Ni(111) and the Boudouard reaction at 3.7 mbar by Near Ambient Pressure X-Ray Photoemission Spectroscopy (NAPXPS), i.e. at one order of magnitude higher pressure than previously explored in-operando conditions. In this regime, CO intercalates under the graphene layer causing its partial detachment from the Ni substrate. The so-obtained high local CO coverage opens the way to CO₂ formation via the Boudouard reaction. Its onset is witnessed by observing physisorbed CO₂ accumulating below the graphene cover. The so-generated additional carbon atoms transform carbide into graphene, causing the expansion of the graphene islands. In addition, CO adsorption occurs on the strongly interacting areas of the graphene layer, confirming previous results obtained by some of us at low temperatures and in ultra-high vacuum conditions.

KEYWORDS

Graphene, Chemistry under cover, Boudouard reaction, Near Ambient Pressure XPS

1. Introduction

Nowadays, graphene (G) growth is routinely obtained on reactive substrates by hydrocarbon dehydrogenation at high sample temperatures. However, the presence of the substrate affects the transport properties of the G layer. In the case of strongly interacting substrates, such as G/Ni [1,2] and G/Ru [3], the Dirac cone is destroyed or shifted, and, consequently, the exceptional mobility of the charge carriers is lost. A promising way to decouple G from the underlying substrate and restore its peculiar electronic properties is the intercalation of atoms [4] and molecules [5], which has been thoroughly investigated.

Confinement of molecules under the G layer is also interesting for sensoristics and catalysis. On the one hand, the change in the electronic properties of graphene can be used as a probe of adsorption [2]; on the other hand, chemical reactions may be affected by the spatial confinement of the reactants. E.g., the G overlayer weakens the interaction between CO and Pt(111), thus reducing the activation barrier for its oxidation [6]. Therefore the interfaces between G and metal surfaces may act as 2D confined nanoreactors, in which catalytic processes are promoted [7]. The feasibility of this approach was also demonstrated for CO oxidation on G-covered Pt nanoparticles [8] and methanation on h-BN-covered Ni nanoparticles [9].

An experimental study of CO intercalation under G/Ni(111) has been recently performed by Wei et al. by Near Ambient Pressure X-ray Photoemission Spectroscopy (NAPXPS) [10,11] in-operando conditions up to 0.1 Torr. Exposure to 5 Torr has been reported as well, but XPS inspection was performed only after the evacuation of the experimental chamber. The authors find that CO intercalation occurs under a complete G layer, with CO ending up mainly at bridge positions with only a minor component at atop sites. Therefore they conclude that, under the G cover, CO behaves similarly on a bare Ni(111) surface under Ultra High Vacuum (UHV) conditions and at room temperature (RT) [12]. Upon annealing, partial deintercalation of CO occurs at ~350 K. Still, a significant amount of intercalated CO persists even after annealing to 473 K. As expected, the initially strongly interacting G layer detaches from the substrate due to intercalation, giving rise to graphene patches characterised by components at a lower binding energy in the XPS spectrum (weakly interacting and detached graphene in the following). More importantly, no additional O-containing species were detected, neither upon CO intercalation nor during the subsequent in-vacuum annealing procedure.

In a recent paper, we presented experiments performed at the Tempo Beamline of the Soleil Synchrotron radiation source, demonstrating that G can be grown on Ni(111) by CO exposure at NAP conditions and at $T=500$ K, i.e. at a temperature significantly lower than the one needed when using hydrocarbons as C source [13]. In that study, we also evidenced the first CO_2 formation via the Boudouard reaction above $T=600$ K. This paper reports on complementary results obtained at the same facility by performing in-operando NAPXPS experiments. In this experiment, a full G/Ni(111) layer is grown by ethene dehydrogenation, and it is exposed to CO at a pressure as high as 4 mbar. We demonstrate that CO intercalates and allows for the onset of the Boudouard reaction already at 340 K, leading to CO_2 accumulation under the G cover. New physics is therefore disclosed by exploring this so far untrodden pressure range.

2. Methods

2.1 Experimental Set-up

The experiments were performed at the TEMPO beamline of the SOLEIL Synchrotron Radiation source (Saint-Aubin, France) with the NAPXPS facility of Sorbonne Université. The experimental setup is described in detail in ref [14], so we only recall the experimental features pertinent to the present work.

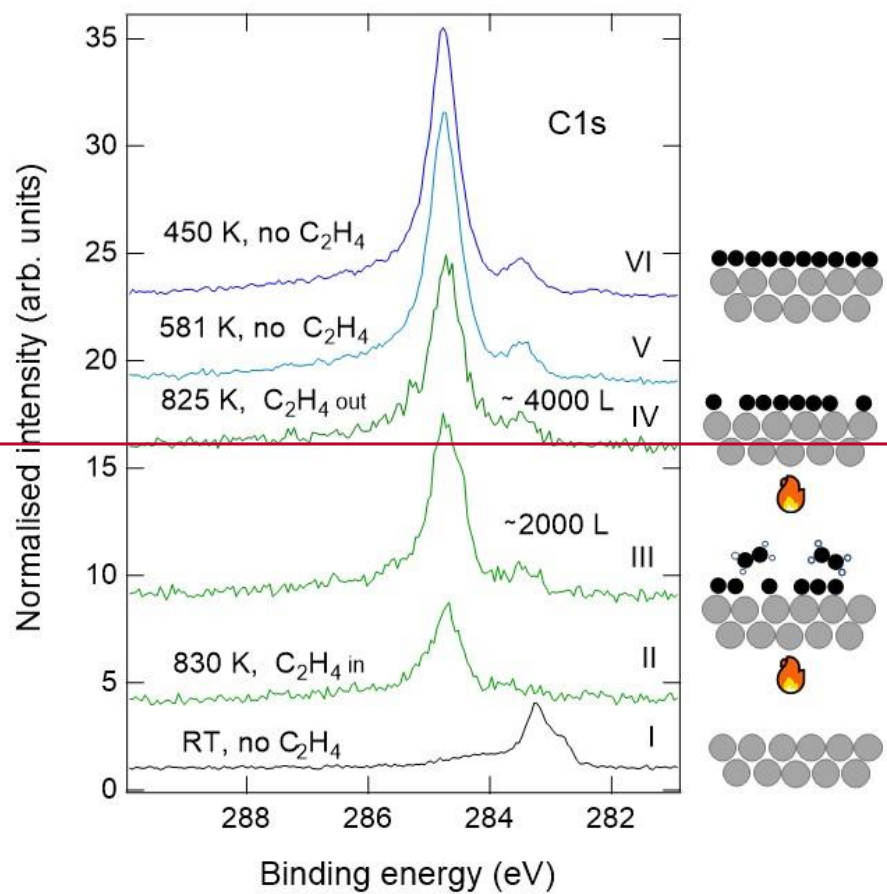
The setup allows measurements from UHV conditions up to 20 mbar. Synchrotron Radiation enters through a differentially pumped stage, forming a beam of 0.1 mm diameter that strikes the sample at an angle of 54° with respect to the surface normal. In NAP conditions, the attenuation of the photoemission signal by scattering off gas-phase CO depends exponentially on the distance between the sample surface and the analyser collimator. Thus the sample is kept at ~ 1 mm distance from the collimator to limit this attenuation. To keep the pressure in the main chamber as constant as possible during NAP experiments, all connections to the pumping systems are sealed by valves. The residual pumping action of nozzle and beam entrance holes is compensated by letting in some CO via a leak valve.

2.2 Sample preparation

The Ni crystal is mounted on a sample holder heated by a ceramic heater module. The Ni(111) surface is cleaned in UHV by sputtering cycles with 3 keV Ar^+ ions followed by annealing to $T\sim 1000$ K and by reactive cleaning in $5\cdot 10^{-7}$ mbar of O_2 at 1000 K for 10 minutes. This procedure led to a surface clean of contaminants but some carbide, which could not be removed entirely.

Graphene was grown by exposing the sample at $T=830$ K to $P=1.7 \cdot 10^{-5}$ mbar of C_2H_4 for 300 s, corresponding to ~ 3800 L, i.e. following the same protocol as in ref. [15].

Selected spectra of the C 1s region recorded during the growth process are shown in Fig. 1. The bottom spectrum (black) corresponds to the surface at RT after completing the cleaning procedure. We note that it still shows some nickel carbide, which could not be removed. The sample is eventually heated to 830 K and exposed to C_2H_4 (green spectra). Then the chamber is evacuated while keeping the sample at 825 K (dark green spectrum), and the latter is eventually cooled down at 450 K under UHV conditions (topmost blue spectrum). The formation of graphene is indicated by the appearance of a peak centred around 284.5 eV. We notice that its intensity is lower at the end of the exposure (dark green trace) than after cooling the sample (blue trace). This indicates that, while most of the G layer forms by ethene dehydrogenation, full monolayer coverage is reached by C segregation during the cooling process. A more detailed inspection of the data shows that the relevant temperature for segregation ranges from $T=830$ K to 580 K, while no further changes occur in the C 1s spectral region at lower T.



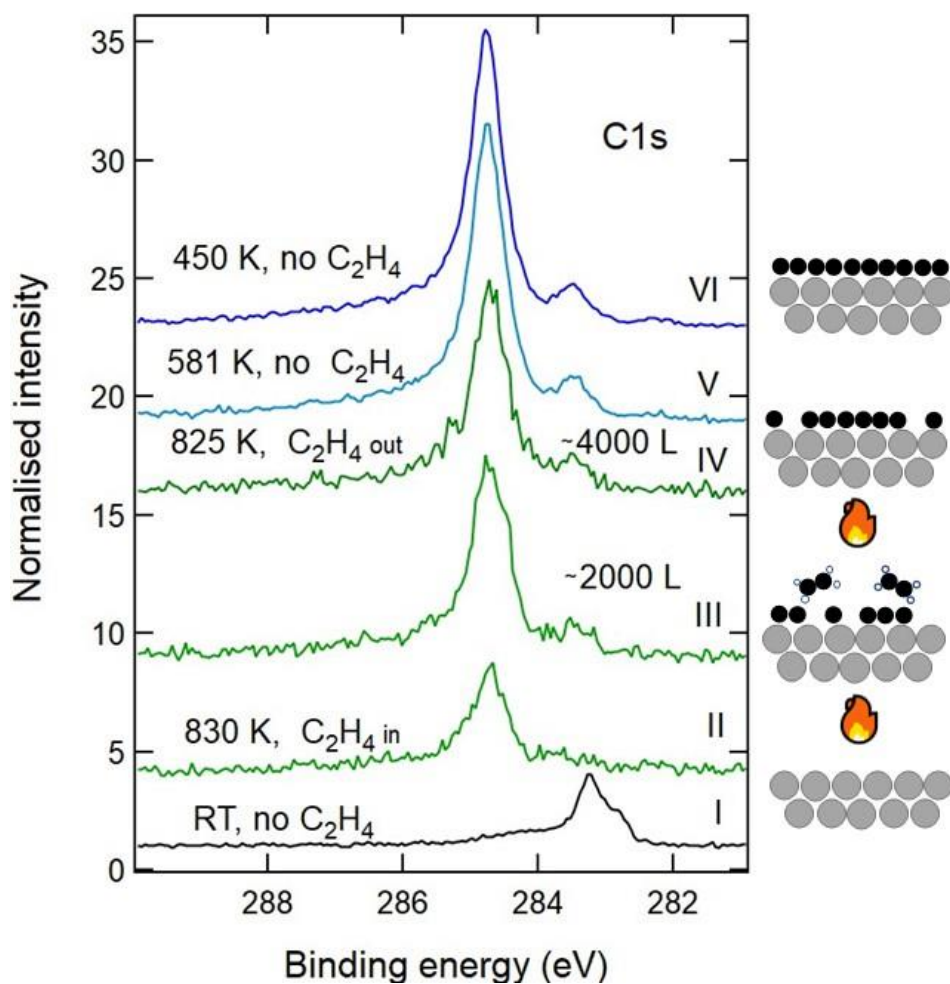


Fig.1 Evolution of the C 1s region during graphene growth by ethylene dehydrogenation. Spectra were recorded with photon energy $h\nu=400$ eV to achieve a high sensitivity to carbon. Intensities are normalised to the background. Spectra are normalized scaling the value of the background in the low binding energy region to 1. From bottom to top: I) Ni(111) surface at RT after the cleaning procedure. Some residual nickel carbide is still present, and it transforms into graphene upon heating between 640 K and 716 K. The low E_b shoulder of the Ni₂C peak is due to a carbon deficient carbide phase [10]. II) Spectrum recorded with the sample at T=830 K, just after admitting C₂H₄ into the chamber. III) Same as II) after about 150 s exposure. IV) Spectrum recorded at T=825 K after the evacuation of the chamber. The total exposure time to ethylene was 300 s. V) Spectrum recorded at 581 K while

Formatted: Highlight

Formatted: Highlight

cooling the sample in UHV. VI) Spectrum recorded at $T=450$ K. The total carbon coverage in VI is $1.45 \text{ ML}_{\text{Ni}(111)}$ (out of which $1.26 \text{ ML}_{\text{Ni}(111)}$ is graphene, and $0.19 \text{ ML}_{\text{Ni}(111)}$ is Ni_2C). The sketches on the right schematise the different stages of the experiment.

2.3 Fitting procedure of the XPS spectra.

Unless otherwise specified, XPS spectra of the C 1s and O 1s regions were performed at the photon energy $h\nu=650$ eV, while $h\nu=970$ eV was used for the Ni 2p region (not shown, recorded for control purpose only).

XPS analysis was performed with the KOL-XPD software. All binding energies (E_b) are calibrated with respect to the Fermi edge of the Ni sample, which was acquired as a reference for each set of experiments. After subtracting a Shirley background, the main C 1s peak (related to graphene) has a strong asymmetry and is therefore fitted with Doniach-Sunjić functions convoluted with a Gaussian. Voigt functions proved sufficient to describe the C1s contributions of CO_2 and of gas phase CO as well as all peaks in the O 1s region. A linear background was used for the O 1s region. All the fitting parameters are detailed in Table S1 of the Supporting Information.

Following previous literature, we considered the C1s intensity as composed of several lines. The corresponding binding energies are collected in Table I and are considered fixed parameters in the present analysis. The C1s region is dominated by the graphene signal. Graphene interacts strongly with Ni(111), and different domains form depending on the relative position of the G lattice with respect to the one of Ni(111) [16]. In the present experimental conditions, top-bridge graphene dominates, while top-fcc and top-hcp domains represent a minor contribution so that their presence hardly affects our conclusions. CO intercalation detaches the layer giving rise to two further graphene species, labelled as weakly and detached graphene in ref. [10]. The shape of the graphene components (Lorentian width=0.23 eV, Gaussian width =0.36 eV, Asymmetry= 0.1- 0.16) was determined from the spectra recorded immediately after graphene growth, where only graphene and Ni_2C are present. It was kept fixed for the analysis of all other spectra.

Further peaks in the C1s region are due to Ni_2C , CO and CO_2 .

CO contributes both to the C1s and to the O1s regions. Following literature [10], we considered CO components corresponding to intercalated CO at top and bridge sites, to weakly adsorbed CO at atop positions on graphene and to CO at bridge sites on Ni_2C ; the C1s and O1s binding energies and desorption temperatures are known for these species. CO at atop sites on Ni_2C was neglected since

its intensity is negligible due to its lower saturation coverage and the extension of the Ni₂C covered areas in our experiment. The width of the O1s components related to CO adsorbed species was taken to be the same and fixed to the value determined for CO on bare Ni(111) (Lorentzian width=0.89 eV; Gaussian width=1.00 eV).

Finally, under NAPXPS conditions, gas-phase CO is observed as well. Its apparent E_b depends on the work function of the sample and allows therefore to determine its change. In accord with the literature [10,17], the width of the O1s peak is larger than the one of the C1s peak. The latter has non-negligible contributions due to the excitation of the internal stretch mode and of its overtones.

Under UHV conditions, the ratio of the O 1s and C 1s peak areas of CO is determined by the corresponding photoemission cross-sections ($\sigma_{C1s}=1.5$ Mb; $\sigma_{O1s}=3.5$ Mb at 650 eV), the transmission function of the analyser being constant over the scanned energy interval.

As in our previous paper [13], in order to fit the O 1s and C 1s regions self-consistently, we firstly determined the intensity of the different O 1s components and fitted the C 1s region eventually by imposing that the C 1s intensity of each adsorbed species, $I_{C1s\ ads}$, satisfies the relationship:

$$I_{O1s\ ads}/I_{O1s\ CO\ gas} = \varepsilon I_{C1s\ ads}/I_{C1s\ CO\ gas} \quad (3)$$

Where ε is the stoichiometry ($\varepsilon=1$ for CO and $\varepsilon=2$ for CO₂), $I_{O1s\ ads}$ is the intensity of the O 1s line of the adsorbed moiety and $I_{O1s\ gas}$ and $I_{C1s\ gas}$ are the intensities of the corresponding gas-phase CO lines.

The photoemission signal in NAPXPS conditions is attenuated due to scattering off gas-phase molecules. Such attenuation depends on the gas density between the sample and the entrance slit to the analyser, on their distance and on the kinetic energy of scattered photoelectrons. During CO intercalation, the sample temperature is varied from 300 K to 550 K, thus modifying the gas density above the sample. The perfect gas law may be applied in the reasonable assumption that, close to the sample where the XPS signal of gas-phase CO is collected, the latter is thermalised at the sample temperature. Despite that, the quantitative correction of the attenuation of the photoemission signal remains somewhat arbitrary: indeed, normalisation with respect to the background intensity, as performed under UHV conditions, is meaningless because also background electrons are affected by scattering off gas-phase molecules.

The following systematic errors may further influence the ratio of the O 1s and C 1s intensities :

- a) photoelectron diffraction for the signal of adsorbed species;

b) a different attenuation of the photoemission signal for adsorbed and gas-phase molecules since the latter are closer to the nozzle so that their photoemission signal is transmitted to the analyser through a shorter path.

c) uncontrolled changes in the position of the sample during annealing and cooling procedures, which may modify the distance between the collimator and the sample.

These effects are difficult to estimate. In the present analysis, we neglect them since they may affect the absolute value of the estimated surface coverage but not the general conclusions of the manuscript.

To *estimate* the coverage of the different species, we assume that the surface is initially entirely covered by graphene and carbide. This assumption is undoubtedly true before CO exposure, when no CO-related signal is observed in the O 1s region (Fig. 2, bottom-right spectrum); indeed, if bare Ni(111) patches were present, they would be rapidly covered by the residual CO molecules present in the gas phase even in UHV conditions. Since a full monolayer (ML) of G and of Ni₂C corresponds to 2 ML and 0.5 ML of C (in ML of Ni(111)), respectively, the fraction of surface area covered by graphene (f_G) and by carbide (f_{Carb}) can be obtained from the intensities I_G and I_{Carb} of the corresponding C 1s lines as follows:

$$f_G = \frac{I_G}{I_G + 4 I_{\text{Carb}}} \quad \text{and} \quad f_{\text{Carb}} = 1 - f_G.$$

The G and Ni₂C coverages (θ_G and θ_{Carb} , respectively) are thus given by $\theta_G = 2 f_G$ and $\theta_{\text{Carb}} = \frac{1}{2} f_{\text{Carb}}$. The coverage of CO and CO₂ is then determined by comparing the corresponding C 1s intensity to the one of the graphene recorded at the same pressure and temperature. Since such species are intercalated, the so-obtained coverage must be further corrected for the attenuation factor of the photoemitted electron yield by the graphene layer ($f_{\text{att}} \sim 2.3$, as determined in ref. [18]). However, some uncertainty remains for lines that cannot be separated, e.g. those corresponding to intercalated CO bonded at atop Ni(111) sites and weakly bonded CO adsorbed at atop graphene sites. A reasonable procedure to disentangle these contributions will be discussed in the following.

Under NAP conditions, photoemission peaks due to the gas-phase species also enables tracking of the work function changes of the sample ($\Delta\phi$) by comparing the apparent E_b shifts of such species. Indeed, the change in the binding energy of the Fermi Level ($\Delta(E_{b \text{ FL}})$) is proportional to $-\Delta\phi$ by:

$$\Delta\phi = -K \cdot \Delta(E_{b \text{ FL}} (\text{gas- phase})) \quad (4)$$

with K being a constant close to unity [19]. This relationship holds because the E_b of the gas-phase species is plotted with respect to the Fermi edge of the sample and the inspected gas-phase molecules are at the same potential as the surface due to the focal properties of the analyser

3. Results and discussion.

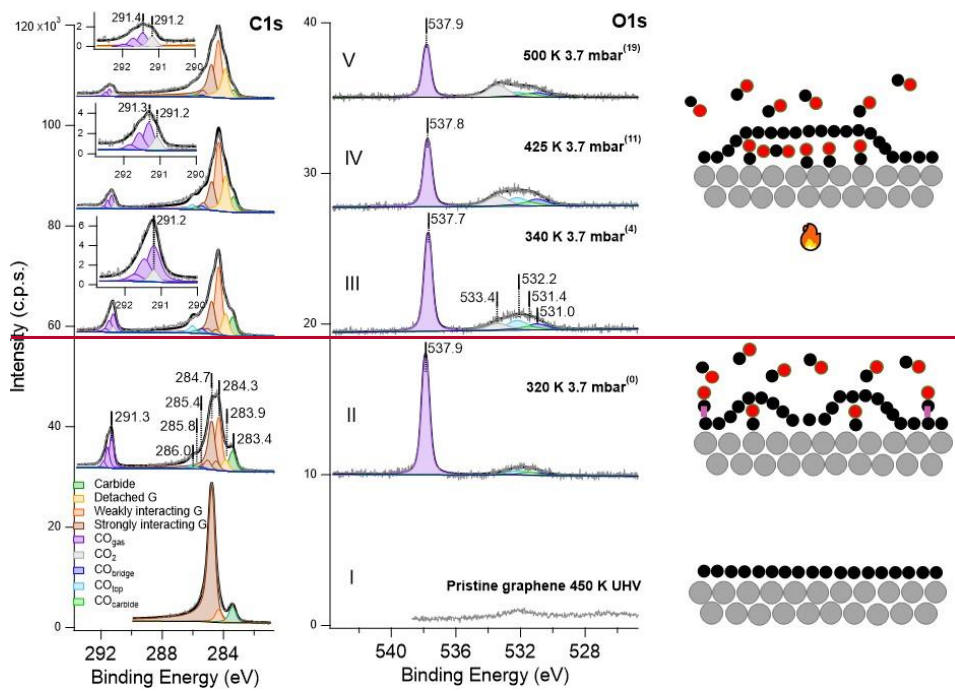
Fig. 2 shows sample spectra of the C 1s (left panel) and O 1s (right panel) regions recorded before and during exposure of the graphene-covered Ni(111) to CO. The pressure is set at 3.7 mbar and decreased by less than 10% during the experiment. Table 1 summarises the binding energies of the different components emerging from the fitting procedure with their assignment.

It is apparent that:

- a) Before introducing CO into the experimental chamber, oxygen is present only in trace amounts on the sample (at most 0.02 ML, see spectrum I-right). The corresponding C 1s region shows features at 284.7 eV and 283.4 eV, related mainly to strongly interacting graphene and Ni₂C, respectively, with only a minor contribution at 284.3 eV due to weakly interacting graphene.
- b) Spectra II to V are significantly modified by introducing 3.7 mbar of CO into the experimental chamber since peaks due to gas-phase CO appear in O 1s and C 1s regions around 537.9 eV and 291.3 eV, respectively. The binding energies of these peaks change during the experiment due to the variation of the work function of the sample. The asymmetric shape of the C 1s feature (see insets in Fig. 2-left) is due to the presence of vibrational overtones.
- c) Upon introduction of CO, a broad structure, due to the convolution of new peaks at 531.0 eV, 531.4 eV and 532.2 eV, forms in the O 1s region already at 320 K (spectrum II). Also, the shape of the corresponding C 1s spectrum changes and can be deconvolved into components corresponding to different types of graphene and CO at different adsorption sites (see table I). Following refs. [10,13], we assign the O 1s lines at 531.0 eV and 531.4 eV to bridge-bonded CO intercalated under the graphene layer and to CO at Ni₂C patches, respectively. The corresponding C 1s lines at 285.4 eV and 285.8 eV overlap with the tail of the intense graphene features. The O 1s component at 532.2 eV and its companion at 286.0 eV are identified with atop CO. The alternative assignment of the 532.2 eV peak to OH contamination is ruled out since it should be coupled to the presence of water molecules in the gas-phase. However, no gas-phase H₂O signal is detected at $E_b(\text{O } 1s)=536.0$ eV [20] in the NAPXPS spectrum. Indeed the intensity at that binding energy is less than 1% of that of

gas-phase CO. Water intercalation followed by dissociation is not possible at such low partial pressures. The C 1s components at 283.9 eV and at 284.3 eV are due to detached and weakly interacting graphene, respectively [10,21]

- d) Upon annealing above 340 K (spectrum III), weakly interacting graphene becomes dominant over the strongly interacting one; also, the detached graphene component increases in intensity.
- e) Finally, a new feature grows at 533.4 eV and becomes prominent over the other O 1s components for $T \geq 425$ K (spectra IV and V). This species is accompanied by the appearance of a C 1s line at 291.3 eV, which partly overlaps with the signal due to gas-phase CO. We assign it to physisorbed CO₂ [13]. Given its low adsorption energy, it must be trapped under the graphene cover in order not to desorb at the temperature of the present experiment. We suggest that it is produced by the Boudouard reaction.



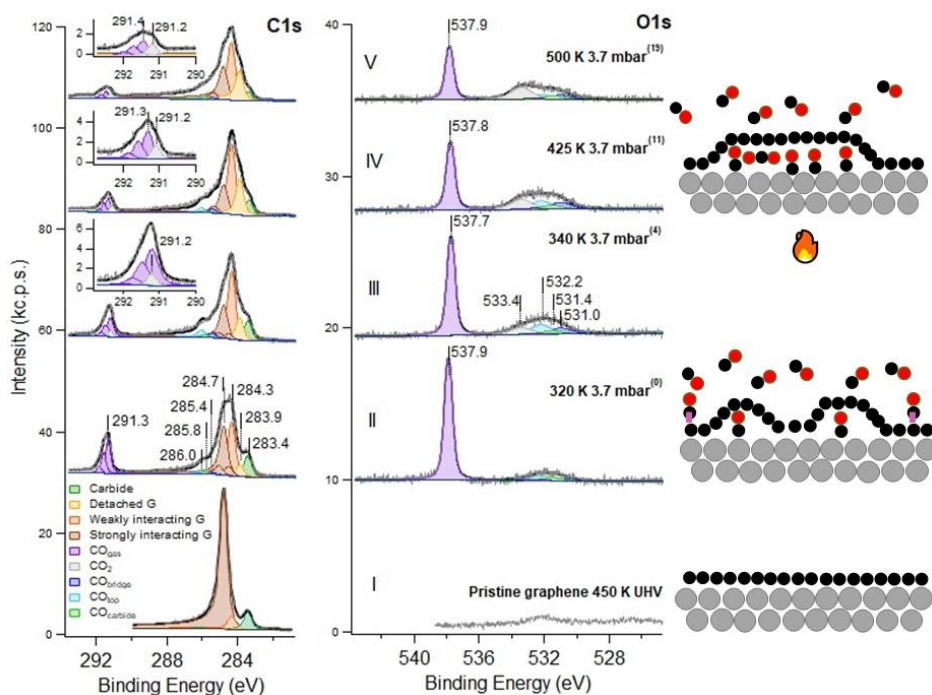


Fig. 2 NAPXPS spectra of the C 1s (left) and O 1s (right) regions for G/Ni(111) in UHV (bottom spectra) and under $P_{\text{CO}} \sim 3.7$ mbar and increasing T. $h\nu = 650$ eV for all spectra except I-left, for which $h\nu = 400$ eV. The spectra are presented without normalisation and upshifted for the sake of clarity. Note the different scales in the two panels. All the components contributing to strongly interacting graphene (top-fcc, top-bridge and the minor contribution of top-hcp) are evidenced by brown filling. The small signal present around 532 eV before intercalation is most likely due to traces of OH. Note that the photoemission intensity is strongly attenuated after filling the chamber with CO so that the intensities recorded in UHV and in the presence of gas-phase CO cannot be directly compared. The small number in each caption of the left panel indicates the corresponding point of the sequence in Fig. 3. Drawings on the right side schematise the different phases of the experiment. The purple rectangles indicate the weak bond of CO adsorbed at strongly interacting graphene areas.

Adsorbed/absorbed species	C 1s B.E. (eV)	O 1s B.E. eV)
Nickel carbide (Ni ₂ C)	283.4	-
Detached graphene	283.9	-
Weakly interacting graphene	284.3	-
Strongly interacting graphene		
bridge-top	284.7	-
top-fcc	284.5 ; 285.0	
top-hcp	285.3	
CO bridge	285.4	531.0
CO top	286.0	532.2
CO bridge on Ni ₂ C	285.8	531.4
Physisorbed CO ₂ under G	291.2	533.4

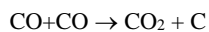
Table I. C 1s and O 1s Binding energies of the different adsorbed species and their assignment, according to refs. [13,16]

The analysis of the data presented in Fig. 2 was performed for all spectra of the series. The outcome is summarised in Fig. 3 vs spectrum number and discussed in the following. The spectra were recorded subsequently at nearly constant CO pressure (~3.7 mbar) while increasing the crystal temperature (see panel E). Panel A shows the evolution of the graphene, carbide and total carbon coverage, while panel B reports the fractional area of the different graphene species and of carbide. Panel C shows the CO and CO₂ coverage obtained, assuming that all the molecules are intercalated underneath graphene. This is not perfectly correct since the atop CO intensity results from the unresolved contributions of intercalated CO at Ni sites and of weakly bonded CO adsorbed at graphene sites, which is not screened by the graphene layer. Since the coverage is corrected for the attenuation of the G cover (roughly a factor of 2.3) for all species, the amount of weakly adsorbed CO on graphene reported in the figure is overestimated by the same factor.

Lastly, the work function change is reported in panel D. We mention that the determination of ϕ for G/Ni(111) is still controversial; values reported in the literature differ significantly, ranging from 3.66 eV [22] to 4.25 eV [23], lower than the one of 4.48 eV measured for free-standing graphene [22]. In our experiment, ϕ increases up to spectrum 7 and slowly decreases afterwards. This behaviour results from the combined effects of the graphene detachment due to CO intercalation and of the presence of weakly adsorbed CO above graphene, as discussed in the following.

We note that the surface fraction covered by strongly interacting graphene ($E_b=284.7$ eV) decreases already from the first spectra and only partially recovers at the highest temperature (panel B). Correspondingly, the weakly interacting ($E_b=284.3$ eV) and detached ($E_b=283.9$ eV) graphene areas initially increase and then remain stable. In literature [1,10], the carbon-containing species with $E_b(C1s)\sim 284.4$ eV is ascribed to weakly interacting graphene. Africh et al. identified this phase with rotated graphene domains sitting above carbide-covered areas [1]; alternatively, it might correspond to the second layer of bilayer graphene patches. Neither explanation seems appropriate to describe the current results: weakly interacting G cannot sit above carbide since the amount of carbide is very small or even missing after G growth by C_2H_4 dehydrogenation. Moreover, weakly interacting G appears promptly upon CO intercalation and grows with the detached graphene component ($E_b(C1s)=283.9$ eV), while carbide coverage decreases. The assignment to a second graphene layer is also problematic since, in this case, the intensity of the strongly interacting G component should remain more or less constant, contrary to our experimental evidence. We thus suggest that CO intercalation proceeds from the edges of graphene flakes and reaction occurs far away from the borders, causing the formation of graphene bubbles in which detached graphene is at the centre and weakly interacting graphene (having an intermediate E_b value between those of detached and strongly interacting graphene) is at the borders.

The total carbon coverage increases by about 0.25 ML (see Fig. 3A) with increasing temperature due to the growth of the fractional area covered by graphene at the expense of the one covered by carbide. The carbide carbon content (estimated as ~ 0.09 ML) is insufficient to account for this change. However, the formation of CO_2 , occurring already at 340 K (panel C), is indicative of the onset of the Boudouard reaction:



which also provides additional carbon. The estimated amount of CO_2 (~ 0.05 ML) can thus justify at least part of it. We note that it is not possible to have a more precise agreement due to the difficulties in the absolute coverage calibration of the adsorbed species; on the other side, the observed CO_2 signal might correspond to the equilibrium coverage between CO_2 production and deintercalation. The carbon production by the Boudouard reaction could thus be underestimated. This hypothesis is supported by the fact that the CO_2 signal promptly decreases when the chamber is evacuated (see Fig. 7).

According to literature, the E_b value of gas-phase CO_2 is expected at ~ 537 eV and 293.6 eV in the O 1s and C 1s regions, respectively [24,25]. Indeed, a small signal at this binding energy is sometimes

present in the C 1s region (not shown), but the corresponding O 1s peak never emerges in XPS spectra. Since the noise level in the O 1s region is typically 4% of the O 1s intensity of gas-phase CO (at $P_{\text{CO}} \sim 3.7$ mbar), we conclude that the partial pressure of gas-phase CO₂ cannot exceed 0.15 mbar, implying that the Boudouard reaction rate is lower than 4% in our conditions. However, such reactivity is sufficient to generate the detected coverage of physisorbed CO₂ under the graphene cover and to provide the required amount of carbon.

The Boudouard reaction mechanism implies dissociation of CO and fast removal of the so obtained O atom by another CO molecule [26]. The rate-limiting step is indeed the dissociation of CO, for which process an activation barrier of about 1.5 eV was estimated theoretically [27]. UHV experiments reported a much lower apparent activation energy of (0.13 ± 0.07) eV/molecule for the Boudouard reaction on Ni(111) [28]. At the same time, Fowles et al. estimated an activation barrier of 1.1 eV/molecule for the rate-limiting step by the carbon formation rate on a commercial catalyst (and at a pressure higher than in the present study) [29]. Whatever its actual value, the reaction barrier must be lowered under graphene cover due to the decrease of the CO adsorption energy. According to recent DFT calculations, such quantity varies from -2.24 eV/molecule on bare Ni(111) to -0.34 eV/molecule under the G cover for a CO coverage of 0.14 ML, while at 0.5 ML the reduction goes from -2.26 eV/molecule to -1.78 eV/molecule [2]. These arguments prove that the occurrence of the Boudouard reaction under graphene cover is more likely than without it, thus supporting our experimental evidence.

We also mention that possible alternative C sources, e.g. the occurrence of CO dissociation or C segregation from the bulk, can safely be excluded. First of all, the absence of atomic oxygen (expected at ~ 529.7 eV [17]) or nickel oxide (expected at ~ 530.3 eV [17]) signals in the O 1s spectrum rules out that the additional carbon is generated by CO dissociation at defects. Indeed, given the high CO pressure, the oxygen released by such a process could be efficiently removed by reaction with further CO. Still, CO oxidation on Ni(111) occurs only at high atomic oxygen coverage while it is endothermic at low oxygen coverage [30]. At 1/3 ML, the reaction has an activation barrier of 0.83 eV [31], while low-temperature oxidation is possible in the presence of weakly bonded atomic oxygen. Also, segregation from the bulk is excluded since the G growth by this mechanism does not take place below 580 K (see discussion of Fig. 1). We can thus safely conclude that the formation of the additional carbon is due to the Boudouard reaction.

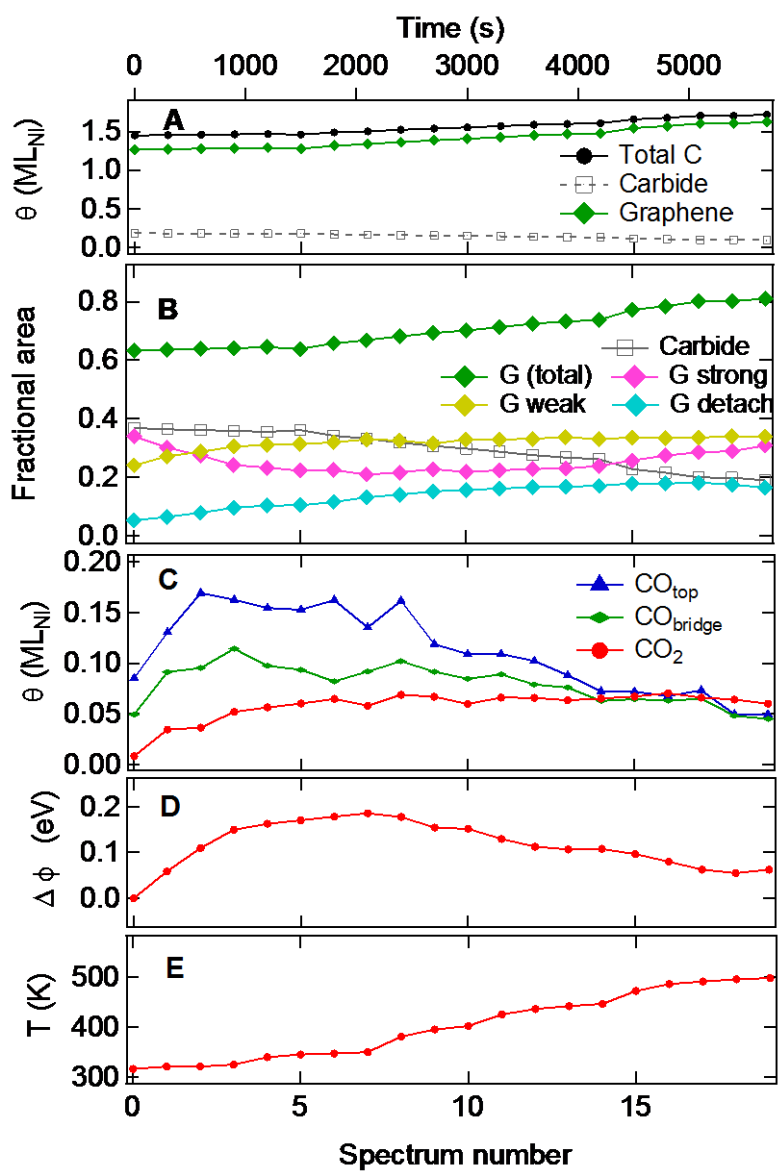


Fig. 3. Analysis of the data reported in Fig. 2. The abscissa refers to the number of subsequent spectra recorded in the experimental run. A) Graphene, carbide and total carbon coverage. B) Fractional area of the different graphene species and carbide. The procedure used to calculate these values (explained in the experimental section) assumes that the surface is entirely covered by graphene or carbide. C)

Coverage of atop- and bridge-bonded CO and of CO₂. D) Variation of the average work function. E) Sample temperature.

Fig. 3C shows that the coverage of CO molecules adsorbed both at top and bridge sites (CO_{top} and CO_{bridge}, respectively) increases rapidly upon CO exposure and decreases eventually with rising temperature. CO_{top} is initially more abundant, but at the highest T, the coverage of the two species becomes comparable. On the contrary, the CO coverage increases when the sample is cooled to 320 K, under which conditions the atop species dominates over the bridge one (see Fig. 6).

To explain this complex behaviour, we recall that both intercalated CO adsorbed at Ni(111) top sites and on-surface CO adsorbed at G top sites contribute to the 286.0 eV component. They cannot be directly resolved in the XPS spectra, but they are characterised by different thermal stability. To estimate the different contributions to the CO_{top} coverage of intercalated and on-surface CO, we start considering the equilibrium coverage (Θ) vs T for CO adsorbed on bare Ni(111) (Fig. 4, black curve) and on G/Ni(111) (purple curve) at a CO pressure of 3 mbar. Θ is obtained by equating the desorption and the adsorption rates (see Supporting online material), including the coverage dependence of the adsorption energy to improve the accuracy of the estimate. The theoretical curve for the equilibrium coverage of CO on Ni(111) is then calculated from calorimetric data [32] using a parabolic interpolation for $E_{\text{des}}^{\text{bare Ni}}(\Theta)$. For weakly adsorbed CO on G/Ni(111), a linear dependence was assumed for the desorption energy for $E_{\text{des}}^{\text{COweak}}(\Theta)$ with the initial value and the slope estimated in ref. [33]. It is apparent that desorption of weakly adsorbed CO on graphene must occur at a much lower temperature than deintercalation of CO bound to Ni(111). The decrease of the CO_{top} intensity observed in Fig. 3C must then arise mainly from the desorption of the weakly adsorbed moiety.

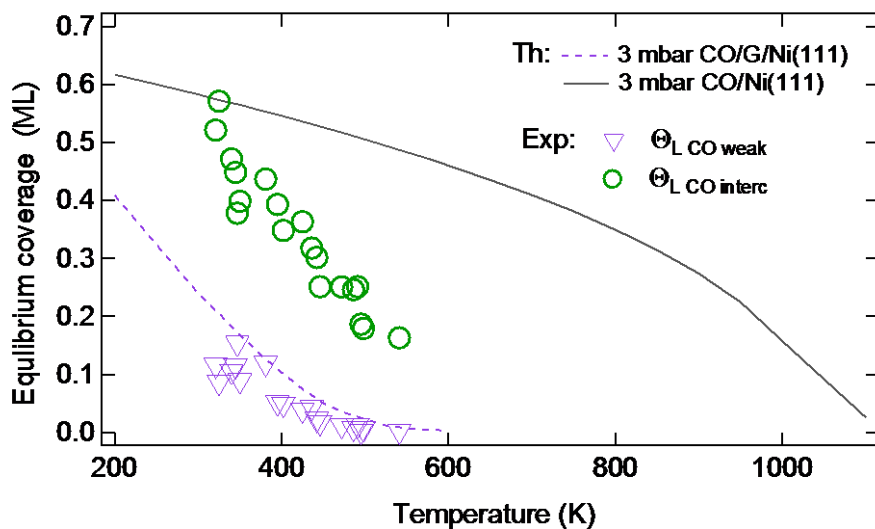


Fig. 4 Estimated equilibrium coverage of CO on Ni(111) (using the calorimetric data of ref. [32] – black curve) and for weakly adsorbed CO on G/Ni(111) (purple dashed curve - [33]). They are compared with the *local* CO coverage observed for the weakly bonded (CO_{weak}) species on graphene and the intercalated ($\text{CO}_{\text{interc}}$) one.

The variations of ϕ during the experiment (Fig. 3D) support this conclusion. In fact, its initial increase can be explained both by the adsorption of CO on graphene and by the detachment of graphene due to CO intercalation. Both effects induce a change of the same sign. On the contrary, the slow decrease observed after scan 7 is unexpected considering that, the relative amount of weakly and detached graphene increases in this temperature range, and the one of strongly interacting graphene is about constant. Therefore, the observed behaviour can be rationalised only by the desorption of weakly adsorbed CO *above* graphene.

At 500 K, only intercalated CO is stable. In this condition, we observe a comparable signal for atop and bridge bonded CO. This result is at variance with literature for the same system [2,10] and for CO on bare Ni(111) [12], for which $\text{CO}_{\text{bridge}}$ is dominant. However, on bare Ni(111), a comparable population of CO at top and bridge sites was reported by Infrared Reflection Absorption Spectroscopy for the compressed 0.57 ML phase obtained in UHV at 80 K [34]. On the contrary, little or no CO at top sites is detected experimentally for G/Ni(111) [2,10], and *ab-initio* calculations [2] predict that this species is not stable under cover. At variance with the cited papers, our experiments were

performed in-operando conditions, i.e. recording the XPS spectra in CO pressure and for $RT \leq T \leq 500$ K. Having already ruled out the possibility that the 532.2 eV signal is related to OH species, we tentatively explain the different outcome of our study with the different experimental conditions. We also mention that theoretical calculations in ref. [2] were performed for a fully detached graphene layer while, in our experiment, a mixed layer consisting of patches of strongly interacting, weakly interacting and detached graphene is present. Therefore, the situation is more complex since the coverage of intercalated CO is not uniform on the surface and areas of high local coverage of intercalated CO coexist with areas where no intercalation takes place, and CO weakly adsorbs at RT under NAP conditions. We suggest, therefore, that the total energy of such a mixed layer can be lower than the one of a fully detached layer with only bridge-bonded CO. Indeed, at high local coverage, the adsorption energy of CO under G is calculated to be around -1.7 eV/molecule, to be compared to -2.1 eV/eV molecule on bare Ni [2]. The difference, which accounts for the energy cost of detaching the graphene layer, is indeed comparable with the adsorption energy of weakly adsorbed CO above graphene, estimated experimentally to be around 0.35 eV/molecule at 1/3 ML coverage and even higher at lower coverage [33]. This explains why, despite the higher pressure with respect to previous studies [2,10], we do not observe complete delamination of the graphene layer. We speculate that in such a mixed layer, also atop CO can be stable under graphene bubbles given the high local coverage.

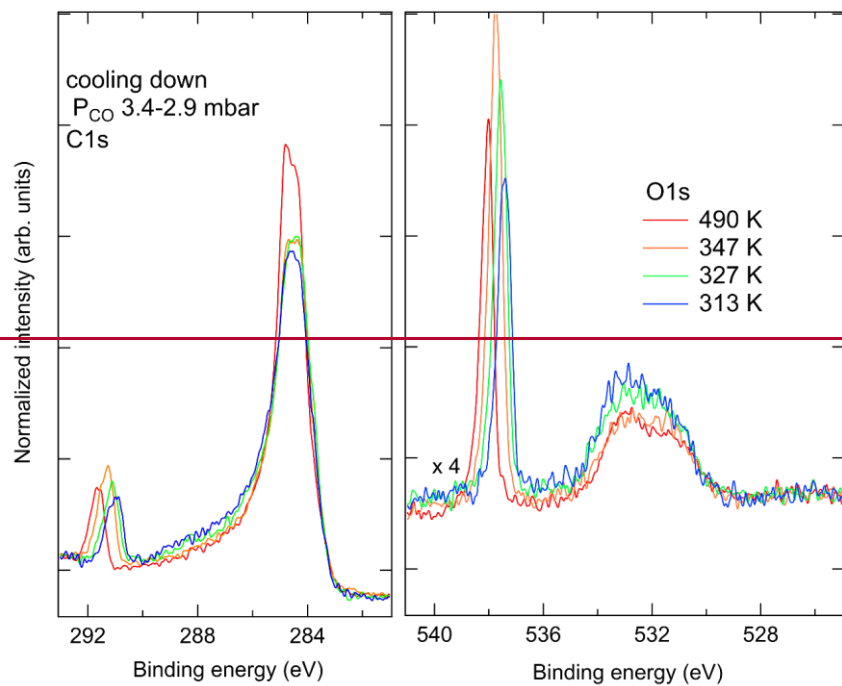
Considering that intercalated CO is present only under detached or weakly interacting graphene areas, which cover about half of the sample, we estimate a local CO coverage of ~ 0.5 ML around RT (though it may be different under the weakly and detached G areas). Such high local coverage may allow populating of a compressed phase in which both top and bridge sites are occupied in comparable amounts under dynamical equilibrium conditions, as in the case of bare Ni(111) at low temperature and in UHV [34].

To determine the fraction of non-intercalated atop CO, we assumed that the coverage of atop and bridge CO under cover are comparable at any T, as is indeed the case at high temperatures. The total coverage of intercalated CO (Θ_{COinterc}) is then twice the one of bridge CO. The coverage of CO weakly adsorbed on graphene (Θ_{COweak}) and overlapping with intercalated CO at atop sites can then be estimated by the difference between the intensity of atop and bridge bonded CO after removing the correction for the attenuation factor $f_{\text{att}} \sim 2.3$ due to graphene, which should be applied only to the intercalated species. Since CO binds only to strongly interacting graphene [33], the *local* coverage of CO_{weak} ($\Theta_{\text{L COweak}}$) can be obtained by dividing Θ_{COweak} by the fractional area occupied by strongly interacting graphene. The resulting coverage is shown by the violet triangles in Fig. 4, which are indeed in good agreement with the expected equilibrium $\Theta_{\text{L COweak}}$. Similarly, the *local* coverage of

intercalated CO ($\Theta_{L\ CO_{interc}}$) may be estimated by dividing $\Theta_{CO_{interc}}$ by the total fractional area occupied by weakly adsorbed plus detached graphene (circles in Fig. 4). It is apparent that $\Theta_{L\ CO_{interc}}$ decreases with temperature more rapidly than expected for CO/Ni(111). This high desorption/deintercalation rate could indicate partial conversion into CO₂ and/or lower adsorption energy under cover. Indeed, for the similar system CO/Pt(111), the latter quantity decreases from 1.74 eV/molecule to 1.21 eV/molecule when CO is intercalated under G/Pt(111) [6].

Note that if the amount of intercalated atop CO were smaller, the relative amount of weakly adsorbed CO would be even higher. A constraint on the maximum amount of weakly adsorbed CO is provided by the intensity of the 532.2 eV remaining after the evacuation of the chamber (see Fig. 7 below), which can only be due to intercalated CO at atop sites.

Further identification of weakly bonded CO on G/Ni(111) is provided by the experiment reported in Fig. 5. Starting from a G/Ni(111) sample with intercalated CO, we slowly decreased the temperature from 490 K to 313 K at nearly constant CO pressure. Upon cooling, the O 1s features related to adsorbed species increase in intensity while the main C 1s peak decreases and a shoulder grows on its high energy side. Both the C 1s and O 1s peaks related to gas-phase CO downshift with cooling, indicating an increase in work function. Considering that, the relative amount of strongly interacting, weakly interacting and detached graphene remains nearly constant in this T range, the work function variation can only be induced by CO adsorption at G/Ni(111). Since this is the only change in the system, it must also be responsible for the enhanced asymmetry of the C 1s line of graphene.



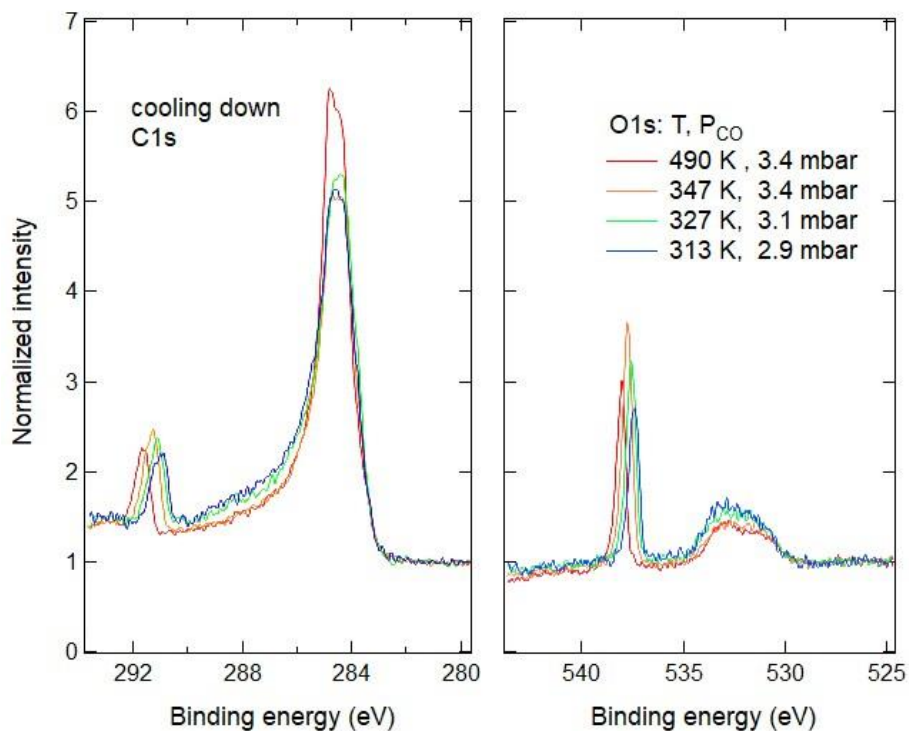


Fig. 5. C 1s (left) and O 1s (right) XPS spectra recorded while cooling the sample from 490 K to 313 K in $P_{CO} \sim 3.1$ mbar. The C 1s and O 1s spectra are normalized scaling the value of the background in the low binding energy region to 1. spectra are normalised on the area of the G-related peaks between 283 eV and 290 eV. O 1s spectra are normalised on the background and multiplied by a factor 4 for better visualization. The same data spectra are fitted in Fig. S1 without normalization.

Formatted: Highlight

Formatted: Highlight

Formatted: Highlight

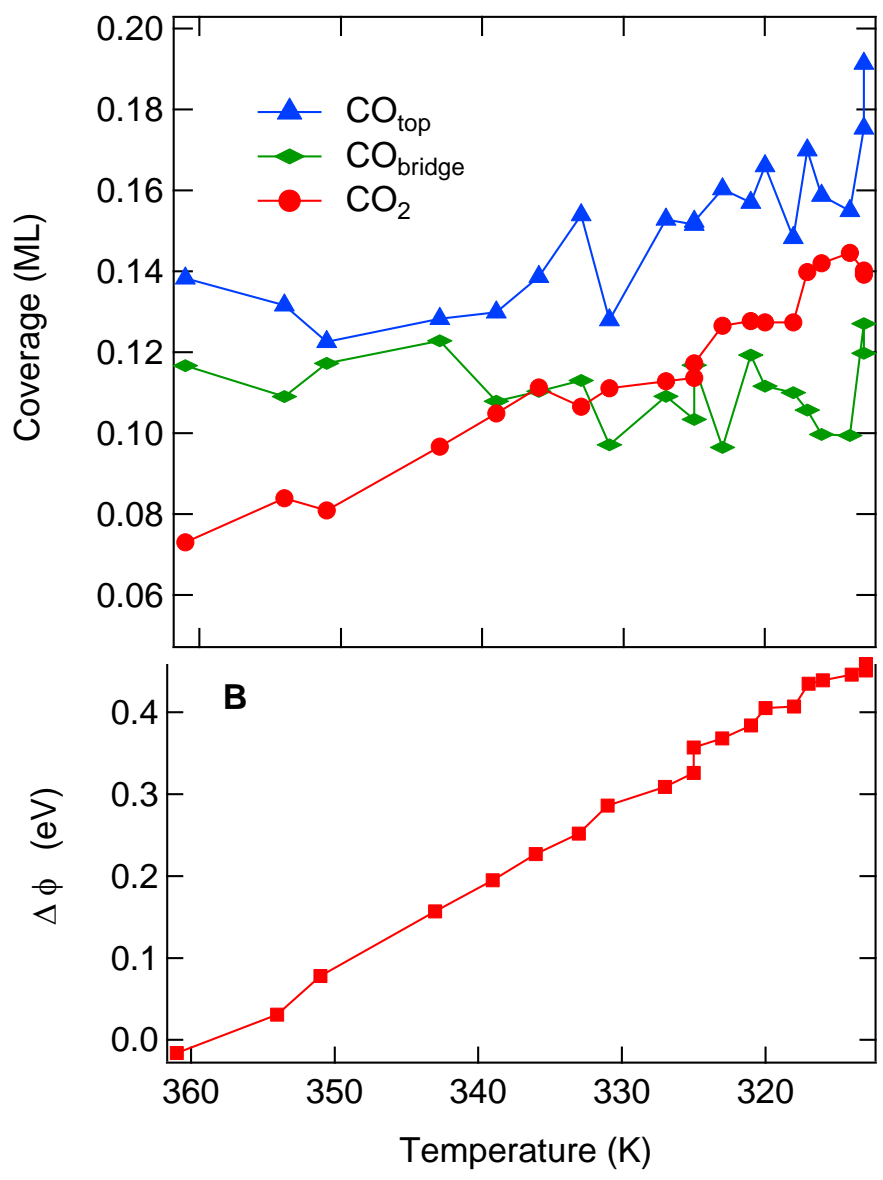


Fig. 6 Analysis of the whole sequence of spectra of the experiment in Fig. 5. A, in which the sample was cooled down in a constant CO pressure $P_{CO} \sim 3.1$ mbar. A): Coverage of CO_{bridge} (green lozenges), CO_{top} (blue triangles) and CO₂ (red circles) vs T. B) Work function variation vs T. Note the reversed scale of the X-axis, corresponding to the cooling process.

In Fig. 6, the coverage of the different CO species is deduced from fitting the O 1s region (see Fig. S1) and the work function change $\Delta\phi$ are plotted vs sample temperature. The CO_{top} coverage increases for $T < 340$ K, while $\text{CO}_{\text{bridge}}$ remains nearly constant over the whole T range. In addition, the amount of physisorbed CO_2 present under cover, corresponding to the O 1s component at 533.4 eV, grows almost linearly with decreasing T. This is in apparent contradiction with the increase of the CO_2 signal observed when heating the sample. The overall picture can be rationalised by reminding that CO_2 formation needs a considerable amount of intercalated CO, which is only present after the detachment of a significant fraction of the graphene layer. Therefore, in the annealing sequence, the CO_2 signal arises from the combination of two competing effects: the rate of the Boudouard reaction (decreasing with increasing T) and the area of detached and weakly interacting graphene (larger at higher T). When cooling down, on the contrary, it is uniquely determined by the increase of the equilibrium constant of the Boudouard reaction since the catalytically active area (proportional to the amount of detached/weakly interacting graphene) remains constant.

Finally, we remark that the 533.4 eV line can only be due to physisorbed CO_2 under cover. Indeed, the alternative identification with transient water contamination has already been ruled out since, given its low adsorption energy, a significant partial pressure of H_2O in the gas-phase would be needed to justify a metastable coverage resulting in such intensity. In this case, the O 1s line of gas-phase H_2O should be visible at ~ 536 eV [20], contrary to experimental evidence. We also exclude that the 533.4 eV peak is due to the formation of tetracarbonyl-nickel since the corresponding feature is missing in the Ni 2p spectrum, at least within our experimental sensitivity (see Fig. S3). Such a signal would indeed be expected given the cross-section for Ni 2p at $h\nu=970$ eV and the one for O 1s at $h\nu=650$ eV. Moreover, the formation of tetracarbonyl-nickel is expected to be thermodynamically less favoured than the Boudouard reaction because it involves four CO molecules instead of two.

The signal at 533.4 eV disappears when the system is evacuated (see Fig. 7). A direct comparison of the spectra under NAP and UHV conditions is not possible because of the already mentioned attenuation of the signal due to gas-phase CO. To compare the spectra of Fig. 7, we, therefore, proceeded as follows:

1) We assume that the graphene sheet is not affected by the evacuation process. This allows determining the distance d between the sample and the nozzle by

$$I(\text{P}_{\text{CO}}) = I_{\text{UHV}} \exp(-d/\lambda_{\text{CO}})$$

where I_{UHV} and $I(\text{P}_{\text{CO}})$ are the intensity in the absence and in the presence of CO pressure, respectively. The mean free path of C 1s electrons λ_{C1s} is then calculated from the CO gas density and the cross-section for inelastic scattering of electrons having the kinetic energy of C 1s electrons in our experiment (taken from ref. [35] as the difference between the total cross-section and the elastic cross-section).

2) A similar relationship is used to estimate the attenuation of the signal due to O 1s electrons using the corresponding $\lambda_{\text{O 1s}}$ and the distance d .

3) The so-obtained correction factors for the C 1s and O 1s lines are used to rescale the corresponding spectra after subtracting a linear background.

Upon evacuation of the experimental chamber (see Fig. 7 and Fig. S2), both the asymmetry in the C 1s region and the O 1s components due to CO_2 and weakly adsorbed CO disappear. The final intensity of the 532.2 eV component is smaller than the one at 531.0 eV due to bridge bonded CO, which remains almost unaffected. Such behaviour indicates that: i) intercalated $\text{CO}_{\text{bridge}}$ is stable at RT; ii) since the intensity of CO_{top} and $\text{CO}_{\text{bridge}}$ are expected to be equal under CO pressure at RT, the fact that the 532.2 eV component is now smaller indicates that part of the intercalated CO_{top} was metastable and has now de-intercalated. This is coherent with the lower adsorption energy expected for this species; iii) the narrowing of the graphene peak is thereby associated with the decrease of the weakly interacting and detached components.

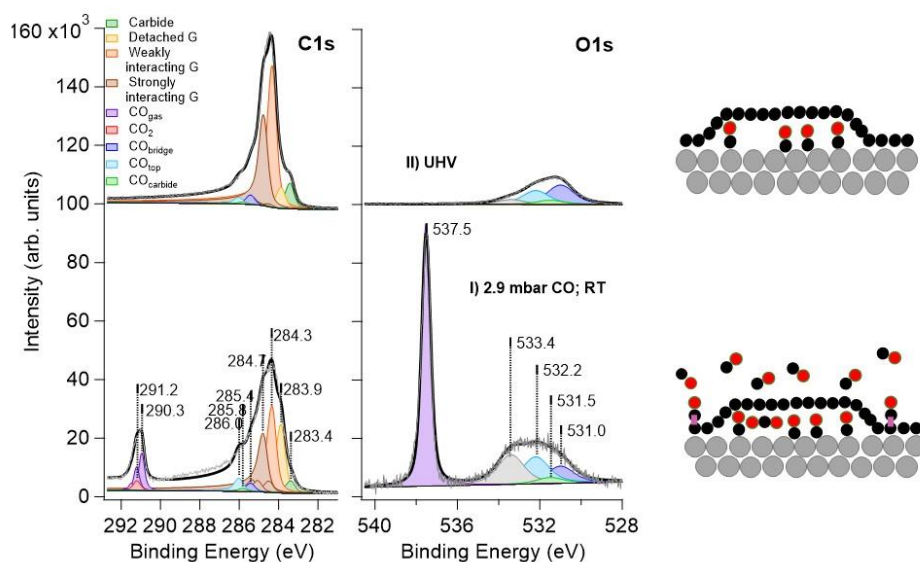


Fig. 7. Comparison of the XPS spectra of G/Ni(111) at $T=313$ K before (bottom, $P_{\text{CO}}=2.9$ mbar) and after (top, UHV) evacuating the experimental chamber. The spectra of the C 1s and of the O 1s region have been corrected for the attenuation due to the gas-phase (see text).

4. Conclusions

We have investigated CO intercalation under G/Ni(111) for so far unexplored in-operando NAP conditions. Our experiments show that:

- CO intercalates below graphene, binding to Ni(111) both at atop and bridge sites, indicating a local coverage of CO higher than the ones observed so far without monitoring the surface in real-time.
- This high local CO coverage enables the formation of physisorbed CO_2 under the graphene cover via the Boudouard reaction already at 340 K. Its accumulation underneath graphene is evident in the NAPXPS spectra. At the same time, the absence of the corresponding gas-phase signal indicates a small reaction probability. The generated carbon converts carbide into

graphene, enlarging the fraction of the graphene-covered surface. To the best of our knowledge, this result is the first demonstration of the occurrence of the Boudouard reaction on Ni(111) under graphene cover already close to RT. Since the reaction rate increases with CO pressure, we expect this result to be relevant under catalytic conditions on nickel-based catalysts involving the presence of gas-phase CO, also as a side product.

- c) CO adsorbs above strongly interacting domains of the G layer. Such results confirm our previous findings obtained in UHV at low temperature [33], from which a relevant equilibrium coverage of CO at RT in the mbar pressure range was predicted. Such weakly bound CO might effectively enable a higher rate for reactions involving CO, thanks to the lower activation barrier.

These conclusions are expected to have an impact on the study of chemical reactions undercover [36] and contribute to filling the pressure gap between previous NAP studies and the real catalytic conditions at even higher pressures.

Acknowledgements

We acknowledge financial support from MIUR through projects PRIN2017 n. 2017NYPHN8 and n. 2017KFMJ8E_003 and from Fondazione Compagnia di S. Paolo through project MC-nano.

G.C. and M.L. acknowledge financial support from the Foundation for Polish Science (First TEAM/2016-2/14 (POIR.04.04.00-00-28CE/16-00) project co-financed by the European Union under the European Regional Development Fund) and the National Science Centre of Poland (OPUS 8 2014/15/B/ST3/02927 project), respectively.

We acknowledge the helpful discussion with Stefano Stranges, Cristiana Di Valentin and Daniele Perilli. We also acknowledge Cristina Africh and Cinzia Cepek for private communications about their experiment.

References

- [1] C. Africh, C. Cepek, L.L. Patera, G. Zamborlini, P. Genoni, T.O. Montes, A. Sala, A. Locatelli, G. Comelli, T.O. Montes, A. Sala, A. Locatelli, G. Comelli, Switchable graphene-substrate coupling through formation/dissolution of an intercalated Ni-carbide layer, *Sci.*

- Rep. 6 (2016) 1–8. <https://doi.org/10.1038/srep19734>.
- [2] S. Del Puppo, V. Carnevali, D. Perilli, F. Zarabara, A.L. Rizzini, G. Fornasier, E. Zupanič, S. Fiori, L.L. Patera, M. Panighel, S. Bhardwaj, Z. Zou, G. Comelli, C. Africh, C. Cepek, C. Di Valentin, M. Peressi, Tuning graphene doping by carbon monoxide intercalation at the Ni(111) interface, *Carbon N. Y.* 176 (2021) 253–261. <https://doi.org/10.1016/j.carbon.2021.01.120>.
- [3] M. Gyamfi, T. Eelbo, M. Waniowska, R. Wiesendanger, Inhomogeneous electronic properties of monolayer graphene on Ru(0001), *Phys. Rev. B - Condens. Matter Mater. Phys.* 83 (2011) 1–4. <https://doi.org/10.1103/PhysRevB.83.153418>.
- [4] A. Dong, Q. Fu, M. Wei, X. Bao, Graphene-metal interaction and its effect on the interface stability under ambient conditions, *Appl. Surf. Sci.* 412 (2017) 262–270. <https://doi.org/10.1016/j.apsusc.2017.03.240>.
- [5] X. Fei, L. Zhang, W. Xiao, H. Chen, Y. Que, L. Liu, K. Yang, S. Du, H.J. Gao, Structural and electronic properties of Pb- intercalated graphene on Ru(0001), *J. Phys. Chem. C.* 119 (2015) 9839–9844. <https://doi.org/10.1021/acs.jpcc.5b00528>.
- [6] Y. Yao, Q. Fu, Y.Y. Zhang, X. Weng, H. Li, M. Chen, L. Jin, A. Dong, R. Mu, P. Jiang, L. Liu, H. Bluhm, Z. Liu, S.B. Zhang, X. Bao, Graphene cover-promoted metal-catalyzed reactions, *Proc. Natl. Acad. Sci.* 111 (2014) 17023–17028. <https://doi.org/10.1073/pnas.1416368111>.
- [7] Q. Fu, X. Bao, Surface chemistry and catalysis confined under two-dimensional materials, *Chem. Soc. Rev.* 46 (2017) 1842–1874. <https://doi.org/10.1039/c6cs00424e>.
- [8] L. Gao, Q. Fu, J. Li, Z. Qu, X. Bao, Enhanced CO oxidation reaction over Pt nanoparticles covered with ultrathin graphitic layers, *Carbon N. Y.* 101 (2016) 324–330. <https://doi.org/10.1016/j.carbon.2016.01.100>.
- [9] L. Gao, Q. Fu, M. Wei, Y. Zhu, Q. Liu, E. Crumlin, Z. Liu, X. Bao, Enhanced Nickel-Catalyzed Methanation Confined under Hexagonal Boron Nitride Shells, *ACS Catal.* 6 (2016) 6814–6822. <https://doi.org/10.1021/acscatal.6b02188>.
- [10] M. Wei, Q. Fu, Y. Yang, W. Wei, E. Crumlin, H. Bluhm, X. Bao, Modulation of Surface Chemistry of CO on Ni(111) by Surface Graphene and Carbodic Carbon, *J. Phys. Chem. C.* 119 (2015) 13590–13597. <https://doi.org/10.1021/acs.jpcc.5b01395>.

- [11] I.P. Prosvirin, A. V. Bukhtiyarov, H. Bluhm, V.I. Bukhtiyarov, Application of near ambient pressure gas-phase X-ray photoelectron spectroscopy to the investigation of catalytic properties of copper in methanol oxidation, *Appl. Surf. Sci.* 363 (2016) 303–309. <https://doi.org/10.1016/j.apsusc.2015.11.258>.
- [12] G. Held, J. Schuler, W. Sklarek, H.-P. Steinrück, Determination of adsorption sites of pure and coadsorbed CO on Ni(111) by high resolution X-ray photoelectron spectroscopy, *Surf. Sci.* 398 (1998) 154–171. [https://doi.org/10.1016/S0039-6028\(98\)80020-4](https://doi.org/10.1016/S0039-6028(98)80020-4).
- [13] R. Davì, G. Carraro, M. Stojkowska, M. Smerieri, L. Savio, M. Lewandowski, J.-J. Gallet, F. Bournel, M. Rocca, L. Vattuone, Graphene growth on Ni (1 1 1) by CO exposure at near ambient pressure, *Chem. Phys. Lett.* 774 (2021) 138596. <https://doi.org/10.1016/j.cplett.2021.138596>.
- [14] H. Liu, A. Zakhtser, A. Naitabdi, F. Rochet, F. Bournel, C. Salzemann, C. Petit, J.J. Gallet, W. Jie, Operando Near-Ambient Pressure X-ray Photoelectron Spectroscopy Study of the CO Oxidation Reaction on the Oxide/Metal Model Catalyst ZnO/Pt(111), *ACS Catal.* 9 (2019) 10212–10225. <https://doi.org/10.1021/acscatal.9b02883>.
- [15] E. Celasco, G. Carraro, M. Smerieri, L. Savio, M. Rocca, L. Vattuone, Influence of growing conditions on the reactivity of Ni supported graphene towards CO, *J. Chem. Phys.* 146 (2017) 104704. <https://doi.org/10.1063/1.4978234>.
- [16] W. Zhao, S.M. Kozlov, O. Höfert, K. Gotterbarm, M.P.A. Lorenz, F. Viñes, C. Papp, A. Görling, H.-P. Steinrück, Graphene on Ni(111): Coexistence of Different Surface Structures, *J. Phys. Chem. Lett.* 2 (2011) 759–764. <https://doi.org/10.1021/jz200043p>.
- [17] E. Monachino, M. Greiner, A. Knop-Gericke, R. Schlögl, C. Dri, E. Vesselli, G. Comelli, Reactivity of carbon dioxide on nickel: Role of CO in the competing interplay between oxygen and graphene, *J. Phys. Chem. Lett.* 5 (2014) 1929–1934. <https://doi.org/10.1021/jz5007675>.
- [18] J. Kraus, R. Reichelt, S. Günther, L. Gregoratti, M. Amati, M. Kiskinova, A. Yulaev, I. Vlassiuk, A. Kolmakov, Photoelectron spectroscopy of wet and gaseous samples through graphene membranes, *Nanoscale.* 6 (2014) 14394–14403. <https://doi.org/10.1039/c4nr03561e>.
- [19] S. Axnanda, M. Scheele, E. Crumlin, B. Mao, R. Chang, S. Rani, M. Faiz, S. Wang, A.P. Alivisatos, Z. Liu, Direct work function measurement by gas phase photoelectron

- spectroscopy and its application on PbS nanoparticles, *Nano Lett.* 13 (2013) 6176–6182.
<https://doi.org/10.1021/nl403524a>.
- [20] D.I. Patel, D. Shah, S. Bahr, P. Dietrich, M. Meyer, A. Thißen, M.R. Linford, Water vapor, by near-ambient pressure XPS, *Surf. Sci. Spectra.* 26 (2019) 014026.
<https://doi.org/10.1116/1.5111634>.
- [21] D. Perilli, S. Fiori, M. Panighel, H. Liu, C. Cepek, M. Peressi, G. Comelli, C. Africh, C. Di Valentin, Mechanism of CO Intercalation through the Graphene/Ni(111) Interface and Effect of Doping, *J. Phys. Chem. Lett.* 11 (2020) 8887–8892.
<https://doi.org/10.1021/acs.jpcclett.0c02447>.
- [22] G. Giovannetti, P. Khomyakov, G. Brocks, V. Karpan, J. van den Brink, P. Kelly, Doping Graphene with Metal Contacts, *Phys. Rev. Lett.* 101 (2008) 026803.
<https://doi.org/10.1103/PhysRevLett.101.026803>.
- [23] E. Del Castillo, S. Achilli, S. Tognolini, E. Fava, S. Ponzoni, G. Drera, C. Cepek, L.L. Patera, C. Africh, E. Del Castillo, M.I. Trioni, S. Pagliara, Surface states characterization in the strongly interacting graphene/Ni(111) system, *New J. Phys.* 20 (2018).
<https://doi.org/10.1088/1367-2630/aae7a0>.
- [24] S. Blomberg, M.J. Hoffmann, J. Gustafson, N.M. Martin, V.R. Fernandes, A. Borg, Z. Liu, R. Chang, S. Matera, K. Reuter, E. Lundgren, In situ x-ray photoelectron spectroscopy of model catalysts: At the edge of the gap, *Phys. Rev. Lett.* 110 (2013) 1–5.
<https://doi.org/10.1103/PhysRevLett.110.117601>.
- [25] T.G. Avval, S. Chatterjee, S. Bahr, P. Dietrich, M. Meyer, A. Thißen, M.R. Linford, Carbon dioxide gas, CO₂ (g), by near-ambient pressure XPS, *Surf. Sci. Spectra.* 26 (2019) 014022.
<https://doi.org/10.1116/1.5053761>.
- [26] D. Hua, G. Li, H. Lu, X. Zhang, P. Fan, Investigation of carbon formation on Ni/YSZ anode of solid oxide fuel cell from CO disproportionation reaction, *Int. Commun. Heat Mass Transf.* 91 (2018) 23–29. <https://doi.org/10.1016/j.icheatmasstransfer.2017.11.014>.
- [27] Y. Morikawa, J.J. Mortensen, B. Hammer, J.K. Nørskov, CO adsorption and dissociation on Pt(111) and Ni(111) surfaces, *Surf. Sci.* 386 (1997) 67–72. [https://doi.org/10.1016/S0039-6028\(97\)00337-3](https://doi.org/10.1016/S0039-6028(97)00337-3).
- [28] H. Nakano, J. Nakamura, Carbide-induced reconstruction initiated at step edges on Ni(1 1 1), *Surf. Sci.* 482–485 (2001) 341–345. [https://doi.org/10.1016/S0039-6028\(00\)01014-1](https://doi.org/10.1016/S0039-6028(00)01014-1).

- [29] J.W. Snoeck, G.F. Froment, M. Fowles, Steam/CO₂ reforming of methane. Carbon filament formation by the Boudouard reaction and gasification by CO₂, by H₂, and by steam: Kinetic study, *Ind. Eng. Chem. Res.* 41 (2002) 4252–4265. <https://doi.org/10.1021/ie010666h>.
- [30] Y. Zhang, X.R. Shi, C. Sun, S. Huang, Z. Duan, P. Ma, J. Wang, CO oxidation on Ni-based single-atom alloys surfaces, *Mol. Catal.* 495 (2020) 111154. <https://doi.org/10.1016/j.mcat.2020.111154>.
- [31] G. Peng, L.R. Merte, J. Knudsen, R.T. Vang, E. Lægsgaard, F. Besenbacher, M. Mavrikakis, On the mechanism of low-temperature CO oxidation on Ni(111) and NiO(111) surfaces, *J. Phys. Chem. C.* 114 (2010) 21579–21584. <https://doi.org/10.1021/jp108475e>.
- [32] J.T. Stuckless, N. Al-Sarraf, C. Wartnaby, D.A. King, Calorimetric heats of adsorption for CO on nickel single crystal surfaces, *J. Chem. Phys.* 99 (1993) 2202–2212. <https://doi.org/10.1063/1.465282>.
- [33] M. Smerieri, E. Celasco, G. Carraro, A. Lusuan, J. Pal, G. Bracco, M. Rocca, L. Savio, L. Vattuone, Enhanced Chemical Reactivity of Pristine Graphene Interacting Strongly with a Substrate: Chemisorbed Carbon Monoxide on Graphene/Nickel(1 1 1), *ChemCatChem.* 7 (2015) 2328–2331. <https://doi.org/10.1002/cctc.201500279>.
- [34] M. Trenary, K.J. Uram, J.T. Yates, An infrared reflection-absorption study of CO chemisorbed on clean and sulfided Ni(111) — Evidence for local surface interactions, *Surf. Sci.* 157 (1985) 512–538. [https://doi.org/10.1016/0039-6028\(85\)90689-2](https://doi.org/10.1016/0039-6028(85)90689-2).
- [35] Y. Itikawa, Cross Sections for Electron Collisions With Carbon Dioxide, *J. Phys. Chem. Ref. Data.* 31 (2002) 749–767. <https://doi.org/10.1063/1.1481879>.
- [36] E.E. Santiso, M.K. Kostov, A.M. George, M.B. Nardelli, K.E. Gubbins, Confinement effects on chemical reactions—Toward an integrated rational catalyst design, *Appl. Surf. Sci.* 253 (2007) 5570–5579. <https://doi.org/10.1016/j.apsusc.2006.12.121>.